CO_2 Capture by Absorption with Potassium Carbonate
First Quarterly Report 2006

Quarterly Progress Report
Reporting Period Start Date: January 1, 2006
Reporting Period End Date: March 31, 2006
Authors: Gary T. Rochelle, Eric Chen, Babatunde Oyenekan, Andrew Sexton, Amorvadee Veawab

April 28, 2006
DOE Award #: DE-FC26-02NT41440
Department of Chemical Engineering
The University of Texas at Austin

Disclaimer

Abstract

The objective of this work is to improve the process for CO_2 capture by alkanolamine absorption/stripping by developing an alternative solvent, aqueous K_2CO_3 promoted by piperazine. The final campaign of the pilot plant was completed in February 2006 with 5m K^+/2.5m PZ and 6.4m K^+/1.6m PZ using Flexipac AQ Style 20. The new cross-exchanger reduced the approach temperature to less than 9°C. Stripper modeling has demonstrated that a configuration with a "Flashing Feed" requires 6% less work that a simple stripper. The oxidative degradation of piperazine proceeds more slowly that that of monoethanolamine and produces ethylenediamine and other products. Uninhibited 5 m $KHCO_3$/2.5 m PZ corrodes 5 to 6 times faster that 30% MEA with 0.2 mol CO_2/mol MEA.

Contents

List of Figures

List of Tables

Introduction

The objective of this work is to improve the process for CO_2 capture by alkanolamine absorption/stripping by developing an alternative solvent, aqueous K_2CO_3 promoted by piperazine. This work expands on parallel bench-scale work with system modeling and pilot plant measurements to demonstrate and quantify the solvent process concepts.

Gary Rochelle is supervising the bench-scale and modeling work; Frank Seibert is supervising the pilot plant. Three graduate students (Babatunde Oyenekan, Ross Dugas, John McLees) have received support during this quarter for direct effort on the scope of this contract. Three students supported by other funding have made contributions this quarter to the scope of this project (Eric Chen – EPA Star Fellowship; Marcus Hilliard, Andrew Sexton – Industrial Associates). Subcontract work was performed at the University of Regina under the supervision of Amy Veawab.

Experimental

Subtask 1.10 describes methods for measuring ionic conductivity, density, and pH of loaded MEA/PZ solutions.

Subtask 2.6 describes methods used in Campaign 4 of the pilot plant.

Subtask 3.1 presents methods for analyzing amine degradation products by anion and cation chromatography.

Task 5 describes methods for electrochemical characterization of corrosion.

Results and Discussion

Progress has been made on five subtasks in this quarter:

Subtask 1.8 – Predict Flowsheet Options

The model in Aspen Custom Modeler was used to model four alternative stripper configurations: matrix, split product, internal exchange and flashing feed at normal pressure and vacuum.

A rate-based model has been developed in Aspen Custom Modeler for a stripper with random packing.

Subtask 2.6 – Campaign 4

Campaign 4 in the pilot plant was completed in early February 2006 and all of the liquid samples have been analyzed for CO_2 loading, piperazine, and potassium. The pilot plant was operated for 12 days on a 24 hour basis for a total of 59 runs. The experiments were conducted 5m K^+/2.5m PZ and 6.4m K^+/1.6m PZ. The absorber and stripper were both packed with a new structured packing, Flexipac AQ Style 20. The newly installed cross-exchanger reduced the approach temperature to less than 10°C. Foaming was observed in the stripper, but perhaps because of hexane left from previous unrelated experiments.

Subtask 3.1 – Analysis of Degradation Products

Liquid samples have been analyzed by cation and anion chromatography from four experiments with MEA and PZ in the degradation apparatus with low gas flow.

Subtask 3.4 – Amine Volatility

Accurate measurements of Water, MEA, and PZ vapor pressure have been made with the high temperature gas FTIR in the pilot plant and in a bench-scale apparatus. These results will be reported in a master's thesis by John McLees in May 2006.

Task 5 – Corrosion

The following tasks were completed.

1) Assembly of a bench-scale electrochemical corrosion setup
2) Validation of electrochemical corrosion setup and experimental procedures
3) Benchmarking corrosion rate and behavior of carbon steel in an aqueous solution of 5 kmol/m^3 (molar) MEA
4) Benchmarking corrosion rate and behavior of carbon steel in an aqueous solution of 5 m. $KHCO_3$/ 2.5 m. piperazine

Conclusions

1. The stripper with a flashing feed requires 6% less work that a simple stripper.

2. With stripping at 30 kPa the mass transfer is 95% liquid film controlled. At 160 kPa it is 70% liquid film controlled at the rich end.

3. Preliminary results show that 5m K^+/2.5m PZ had a lower heat duty as a function of CO_2 removal than 6.4m K^+/1.6m PZ.

4. The new plate and frame cross-exchanger worked very efficiently. The approach temperatures of the 5m K^+/2.5m PZ and the 6.4m K^+/1.6m PZ solvent ranged from 6.9 to 8.9°C and 3.4 to 6.4°C, respectively. The exchanger provided 1.5 to 2.2 transfer units per pass as solvent rate varied from 30 to 12 gpm.

5. Acetate, glycolate, formate, oxalate, nitrite, nitrate have been quantified in both MEA and PZ degradation. Ethylenediamine has been quantified in PZ degradation.

6. The proprietary inhibitor A significantly reduces degradation products from MEA.

7. When dissolved copper is present, MEA degradation produces more formate and less glycolate.

8. The rate of piperazine oxidative degradation is slower than the rate of MEA oxidative degradation.

9. Uninhibited 5 m $KHCO_3$/2.5 m PZ corrodes 5 to six times faster that 30% MEA with 0.2 mol CO_2/mol MEA.

Future Work

We expect the following accomplishments in the next quarter:

Subtask 1.1 – Modify Vapor-Liquid Equilibrium (VLE) Model

A new experimental system will be set up to measure CO_2 VLE with the hot gas FTIR.

Subtask 1.5 – Simulate Base Case Pilot

The absorber data from Campaigns 1, 2 and 4 will be simulated with the spreadsheet model.

Subtask 1.8 – Predict Flowsheet Options

The rate-based model for the stripper will be extended to structured packing and other solvents.

Subtask 1.10 – Simulate MEA Baseline

A master's thesis will be completed by Ross Dugas in May 2006 to fully document the baseline MEA campaign.

Subtask 2.6 – Pilot Plant Campaign 4, Optimization of System Parameters

The material balances for campaign 4 will be reconciled. K_G calculations will be made to quantify and compare the CO_2 absorption performances of the two solvents.

Subtask 3.1 – Analysis of Degradation Products

Four of the unknown peaks from ion chromatography will be identified.

Work will start on the development of a HPLC method for thermal degradation products of MEA and PZ.

Task 1 – Modeling Performance of Absorption/Stripping of CO_2 with Aqueous K_2CO_3 Promoted by Piperazine

Subtask 1.8b – Predict Flowsheet Options and Rate-based Modeling – Aspen Custom Modeler for Stripper

by Babatunde Oyenekan

(Supported by this contract)

Introduction

We have continued to develop the stripper submodel in Aspen Custom Modeler for the overall model of CO_2 absorption/stripping for 7m monoethanolamine (MEA), 5m K^+ / 2.5m PZ and some generic solvents. Previous work suggests that with generic solvents, the optimum ΔH is a function of the stripper configuration used. The vacuum stripper is favored for solvents with $\Delta H_{des} \leq 21$ kcal/gmol CO_2. Since the 5m K^+/2.5m PZ has a lower heat of desorption than 21 kcal/gmol CO_2, the vacuum stripper will be attractive for the solvent. There may be some process configurations that may be quite attractive for the 5m K^+/2.5m PZ solvent. In this quarter, we have evaluated four new stripper configurations (matrix, split product, internal exchange and flashing feed) compared the results obtained to the vacuum stripper at a 5^{o}C approach. This model divides the stripper into sections with Murphree efficiencies assigned to CO_2, water and temperature. A three-parameter expression approximates the equilibrium behavior of the generic solvents. The results show that the flashing feed gives the lowest total equivalent work of all the new configurations at 30 kPa. A rate-based model to predict the operation of real columns has been developed. We present results from the rate-based model for a 5m K^+/2.5m PZ solvent in a pilot plant column with 0.43m inner diameter and a 30 gallons per minute flow rate equipped with IMTP #40 packing. The stripper pressure was varied between 30 and 160 kPa. The results show that the total equivalent work with 90% removal of the CO_2 is minimized at lower operating pressures of the column. The liquid film accounts for 95% of the total mass transfer resistance at 30 kPa and between 81% and 70% at the rich and lean ends of the stripper at 160 kPa.

Experimental (Model Formulation)

Stripper Configurations

Vacuum Stripper

The stripper is operated at 30 kPa and the reboiler runs at 60 – 80^{o}C.

Vacuum stripping has the following features:

1. Lower temperature (less valuable) steam is used to run the reboiler so more electricity can be extracted before the steam is used in the stripper.
2. Additional compression is required for the CO_2.
3. The mass transfer is not as fast as that of the simple stripper because the lower temperature results in slower kinetics.

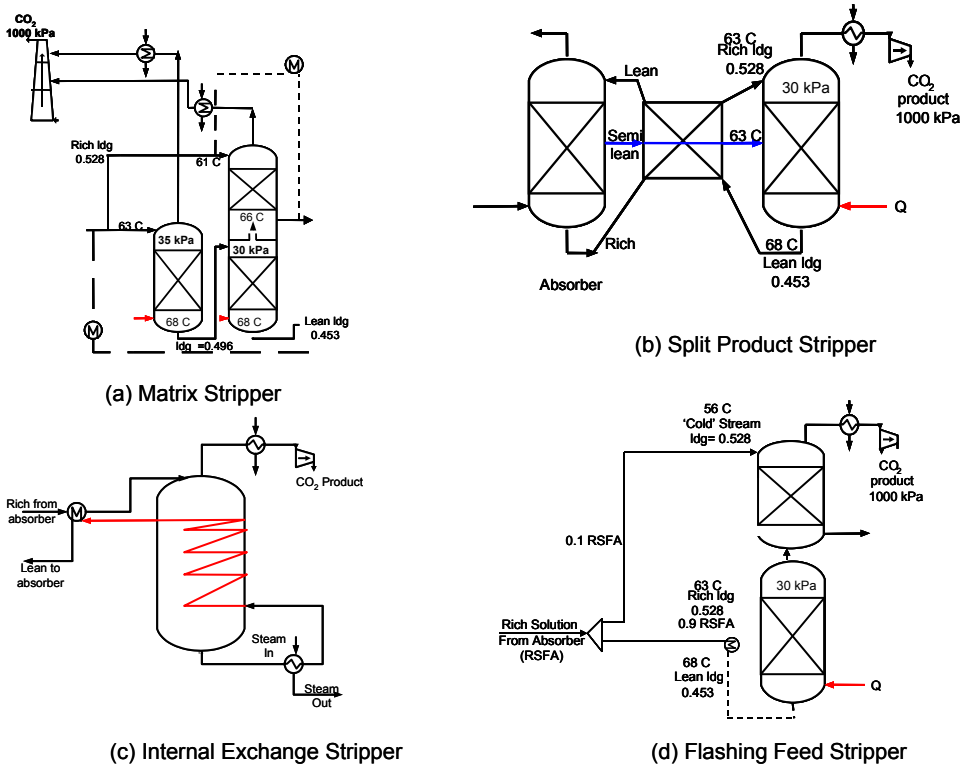

Figure 1: Alternative Stripper Configurations.

Matrix Stripper

The matrix stripper (Figure 1a) is a novel, complex system with number of strippers. As a result of the flow configuration, the effects of temperature change across the stripper are alleviated as with the multipressure stripper, but without the inefficiency of mechanical compression.

Split Product Stripper

With a split product stripper (Figure 1b) semi-lean solution is removed from the middle of the absorber and introduced after cross-exchange to the middle of the stripper.

The rich and semi-lean streams are cross-exchanged to the maximum extent possible before being introduced into the stripper.

Internal Exchange Stripper

Internal heat exchange in the stripper alleviates the effects of temperature change across the stripper by exchanging the hot lean solution with the solution in the stripper. This configuration (Figure 1c) has been described by Leites and Berchenko [1]. One configuration would place continuous heat exchange surface in the stripper so that there is countercurrent heat exchange of the hot lean solution with the solution coming down the stripper.

Flashing Feed Stripper

In this configuration (Figure 1d), the rich stream is split into two, one stream is cross-exchanged with the lean stream leaving the bottom of a stripper while the other is sent to a flash vessel. The split ratio between the 'warm' rich solution and the 'cold' one is 9:1. The vapor leaving this stripper is then contacted with the 'cold' feed in a flash vessel. More CO_2 can be stripped from the 'cold' feed by the vapor stream leaving the main stripper. The reboiler duty for operating the stripper is unchanged and the latent heat of water in the vapor stream leaving the main stripper is used to strip CO_2 from the cold feed.

Aspen Custom Modeler (ACM) Model

Prediction of Stripper Options

A model has been developed in Aspen Custom Modeler to simulate the stripper operation.

Modeling Assumptions

(a) The sections were assumed to be well mixed in the liquid and vapor phases.
(b) The reboiler was assumed to be in equilibrium.
(c) Negligible vaporization of the solvent.

The CO_2 vapor pressure (kPa) under stripper conditions for generic solvents is given by:

$$\ln \quad P_{CO2} = a + (b * ldg) + \frac{\Delta H}{T} \qquad (1)$$

P = the equilibrium partial pressure of CO_2 (kPa)
T = temperature (K)
ldg = mol CO_2/ (mol K^+ + mol PZ) (-)
ΔH = heat of desorption of the solvent (kcal/gmol CO_2)
R is the Universal gas constant (cal/K-mol)

The constant, b, is the inverse of the capacity of the solution. For the 5m K^+/2.5m PZ, the constant, a, was set to 8.82 while the constant, b, was set to 30.69. The ΔH_{des} was set to 15 kcal/gmol CO_2.

The rich CO_2 loading at specified rich P_{CO2} (kPa) leaving the absorber at 40°C for 5m K^+/2.5m PZ is shown in Table 1.

The heat of vaporization of water, partial pressure of water, heat capacities of steam, CO_2 and the solvent (essentially water) were calculated from equation derived from the DIPPR database.

Table 1. Predicted CO_2 Solubility in 5m K^+/2.5m PZ at 40°C

Rich P_{CO2}* (kPa)	**CO_2 loading** $\left[\frac{\text{mol } CO_2}{\text{mol } K^+ + \text{mol PZ}}\right]$
1.25	0.505
2.5	0.528
5	0.551
10	0.573

The partial pressure of CO_2 and water on each section were calculated from equation 8

$$E_{mv} = \frac{P_n - P_{n-1}}{P_n^* - P_{n-1}} \qquad (2)$$

where E_{mv} is the Murphree plate efficiency defined in terms of partial pressures
P_n, P_{n-1} is the partial pressures of the component on sections n and n-1
P_n* is the equilibrium partial pressure of the component leaving section n.

An efficiency of 40% and 100% were assigned to CO_2 and water. The model assumed 100% efficiency with respect to heat transfer.

For a given rich and lean CO_2 loading (corresponding to 90% removal), column pressure and temperature approach in the cross exchanger, the model solves the VLE equations, material and energy balances and outputs the reboiler duty normalized by the moles of CO_2 removed, the equivalent work and the temperature, pressure and concentration profiles in the column.

The equivalent work is a convenient way to quantify the energy requirement of the process. It constitutes the work lost from the turbine upstream of the power plant since the condensing steam used to run the reboiler is no longer available to generate electric power. It also aids in comparing heat and work, which are different forms of energy) on an equivalent basis.

The equivalent work for stripping is given by:

$$W \text{ (kcal/gmol } CO_2) = 0.75\, Q \left[\frac{T_{cond} - T_o}{T_{cond}}\right] + W_{comp} \qquad (3)$$

where Q is the reboiler duty in kcal/gmol CO_2, T_{cond} is the temperature of the condensing steam (temperature of reboiler plus 10K) in the shell of the reboiler and T_o is the temperature of the cooling water (313K). The first term on the right hand side of equation 9 constitutes the amount of work that could be produced if the steam used in running the reboiler were expanded in a Carnot Engine with 75% efficiency. W_{comp} constitutes the adiabatic work of compression of the gas exiting the top of the stripper to 1000 kPa (an arbitrary pressure selected). For this analysis isentropic efficiency of the compressor was assumed to be 75%.

Results and Discussion

Predicted Stripper Performance for Different Configurations

The stripper performance of different configurations to achieve 90% removal, from a rich loading of 0.528 mol CO_2/ (mol K^+ + mol PZ) to a lean loading of 0.453 mol CO_2/ (mol K^+ + mol PZ), corresponding to P_{CO2}* of 2.5 kPa and 0.25 kPa respectively and a 5^{o}C temperature approach are shown in Table 2.

Table 2: Summary of Stripper Performance Using Different Configurations (Rich loading = 0.528, Lean Loading = 0.453, T_{app} = 5^{o}C)

			Energy (kcal/gmol CO_2)			
			Reboiler		Comp	Total
Configuration	P (kPa)	T_{reb} (^{o}C)	Q	W	W_{comp}	W_{eq}
Simple	160	109	41	7.8	1.7	9.4
Flashing Feed	160	109	40	6.0	1.7	7.7
Vacuum	100	97	42	6.8	2.1	8.9
Matrix	150,100	97	47	6.2	2.0	8.2
Vacuum	30	68	50	4.5	3.6	8.1
Matrix	30	68	62	5.0	3.5	8.5
Split Product	30	68	50	4.6	3.6	8.2
Internal Exchange	30	68	46	4.2	3.6	7.8
Flashing Feed	30	68	49	4.0	3.6	7.6

The results show that at 160 kPa, operating the flashing feed configuration offers 18% energy savings when compared to the simple configuration. The matrix stripper offers 8% energy savings when compared to the vacuum stripper at 100 kPa. Of all the configurations at 30 kPa, the flashing feed gives the least equivalent work.

Rate-based Modeling

A rate-based model has been developed in Aspen Custom Modeler to simulate the stripper operation equipped with random packing. This model has the following features:

(a) rigorous thermodynamics is accounted for by an equation regressed from results from the E-NRTL model of Chen et al.[2].

(b) approximate representations of mass transfer with combined reaction.

(c) gas and liquid film mass transfer resistances are taken into account.

(d) Unequal flux of CO_2 and H_2O is accounted for in both phases.

(e) The final pressure of the CO_2 is 1000 kPa. This compression is carried out in five stages with intercooling to 313K.

Modeling Assumptions

(a) The ten sections in to which the packed section is divided are well mixed in the liquid and vapor phases.

(b) The reboiler is assumed to be an equilibrium stage.

(c) There is negligible vaporization of the solvent.

(d) The reaction takes place in the liquid phase.

The CO_2 vapor pressure (kPa) under stripper conditions for the 5m K^+/2.5m PZ solvents is given by Table 3:

Table 3: Adjustable constants in VLE expression.

$$\ln P_{CO2}^{*} = a + b*ldg + \frac{c}{T} + d\frac{ldg^2}{T^2} + e\frac{ldg}{T^2} + f\frac{ldg}{T}$$

A	-10.0863	d	-560390
B	16.91059	e	-5910637
C	-1324.38	f	23418.25

The loadings in terms of total alkalinity at different equilibrium partial pressures of CO_2 at 40^{o}C for 5m K^+/2.5m PZ are given in Table 4.

Some mass transfer calculations were performed using IMTP #40 packing. This is random metal packing with a nominal diameter of 0.04 m, a dry area to volume ratio of 165 m^2/m^3 and a packing factor of 79 m^{-1}. The mass transfer model used was that originally developed by Bishnoi [3] and modified for potassium carbonate/piperazine solution by Cullinane [4]. The model is a rigorous rate model based on eddy diffusivity theory. It integrates a series of differential equations for the thermodynamics in the bulk liquid using the Electrolyte Non-Random Two Liquid (ENRTL) proposed by Chen et al. [1,5-6], diffusion across the liquid film, and reaction in the boundary layer and calculates the liquid-phase mass transfer coefficient with a partial pressure driving force, k_g'. The liquid-phase mass transfer coefficient consists of kinetic and liquid diffusion terms.

Table 4: Loadings at different equilibrium partial pressures of CO_2 at 40°C.

P_{CO2}* (kPa)	**CO_2 loading** $\left[\frac{\text{mol } CO_2}{\text{mol } K^+ + \text{mol PZ}}\right]$
0.125	0.422
0.250	0.448
0.500	0.475
1.000	0.501
1.250	0.510
2.500	0.537
5.000	0.565
10.000	0.593

The flux of CO_2 is given by the expression

$$N_{CO2} = K_G (P_{CO2}^* - P_{CO2}) \quad (4)$$

The overall mass transfer coefficient (K_G) is the sum of the gas phase (k_g) and liquid phase (k_g') components.

$$\frac{1}{K_G} = \frac{1}{k_g} + \frac{1}{k_g'} \quad (5)$$

k_g is obtained from Onda [7] and Wilson [8]. k_g' is calculated by an equation regressed from Cullinane [4]. The liquid-phase mass transfer coefficient with a partial pressure driving force, k_g' is a function of the loading, temperature and partial pressure of CO_2 at the interface.The CO_2 desorption rate is:

$$\text{Rate} = K_G A (P_{CO2}^* - P_{CO2}) \quad (6)$$

The wetted area of contact, A, depends on the equipment and hydraulics in the column.

Predicted Stripper Performance from Rate-Based Model

For a rate-based (non-equilibrium) model the column diameter must be specified. In this work, we have fixed the column diameter to 0.43m, the flow rate of liquid was set at 30 gallons per minute and the height of packing was set to 6m. The rich and lean loading were set at 0.537 and 0.448 mol CO_2/mol Total Alkalinity.

The equivalent work of stripping is calculated as in equation (3). Table 5 shows the total equivalent work obtained for a stripper operating between 30 and 160 kPa with a 10°C

temperature approach in the cross exchanger. The results show that the normalized reboiler duty decreases with increasing pressure from 56 kcal/gmol CO_2 at 30 kPa to 39 kcal/gmol CO_2 at 160 kPa. The total equivalent work appears to go through a minimum at some pressure between 30 and 100 kPa. The general trend however dictates that the equivalent work is lower at lower pressures for a 5m K^+/2.5m PZ solvent which is consistent with our earlier work [9]. This presents opportunities for alternative materials of construction of the stripper. Fiber-reinforced plastic (FRP) could be an alternative material as opposed to carbon or stainless steel.

Table 5: Performance of 5m K^+/2.5m PZ at Different Stripper Pressures (L=30 gpm, Cross-Sectional Area of Column = 0.43m, Packing Height = 6m, Rich loading = 0.537, Lean Loading = 0.448, T_{app} = 10°C)

Pressure (kPa)	Q	Reboiler Duty $W_{eq,heat}$	Compression Work, $W_{eq,comp}$	Total W_{eq}
	kcal/gmol CO_2			
30	56	5.1	3.6	8.7
60	43	5.6	2.7	8.3
100	41	6.6	2.1	8.7
160	39	7.6	1.7	9.3

Table 6 shows the mass transfer coefficients and percent gas phase resistance as the rich and lean ends for a 30 kPa and a 160kPa stripper. The results show that the vacuum (30 kPa) stripper is liquid film controlled. The high-pressure strippers are liquid film controlled though with significant gas phase resistance of 19% and 30% at the rich and lean ends respectively. The mass transfer rates increase by a factor of two, from 2.9 kmol/m^2-s to 5.6 kmol/m^2-s in going from the rich to the lean end for the 30 kPa stripper and from 1.4 kmol/m^2-s to 3.1 kmol/m2-s for the 160 kPa stripper. The rates increase as we go from the rich end (top of the column) to the lean end (bottom of the column) because as the liquid flows down the column, the complexes formed in the absorber are decomposed giving rise to free amine which becomes available for more reaction.

Table 6: Mass Transfer Rate Results For 5m K^+/2.5m PZ at Different Pressures (L=30 gpm, Cross-Sectional Area of Column = 0.43m, Packing Height = 6m, Rich loading = 0.537, Lean Loading = 0.448, T_{app} = 10°C)

	P = 30 kPa		P = 160 kPa	
	Rich End	Lean End	Rich End	Lean End
k_g (kmol/m^2-s)	7.4e-4	9.5e-4	5.9e-4	7.2e-4
$k_{g'}$ (kmol/m^2-s)	2.9e-5	5.6e-5	1.4e-4	3.1e-4
K_G (kmol/m^2-s)	2.8e-5	5.3e-5	1.1e-4	2.2e-4
Percent Gas Resistance	4	6	19	30

In order to understand the internal column operation, McCabe –Thiele plots are used. Figure 2 shows the McCabe-Thiele plot for 5m K^+/2.5m PZ at a rich loading of 0.537 mol CO_2/ mol total alkalinity and lean loading of 0.448 mol CO_2/ mol total alkalinity for a vacuum (30kPa) stripper. The reboiler duty and total equivalent work are 56 kcal/gmol CO_2 and 8.7 kcal/gmol CO_2. The reboiler runs at 68°C. The rich feed is sub-cooled and a good driving force is evident in the column. If the column is run at 160 kPa, the McCabe-Thiele plot for the column operation is shown in Figure 3. Flashing of the liquid feed is observed at the top of the column. There is also an evident pinch at the rich end in which we have three sections of the column in which very little mass transfer occurs.

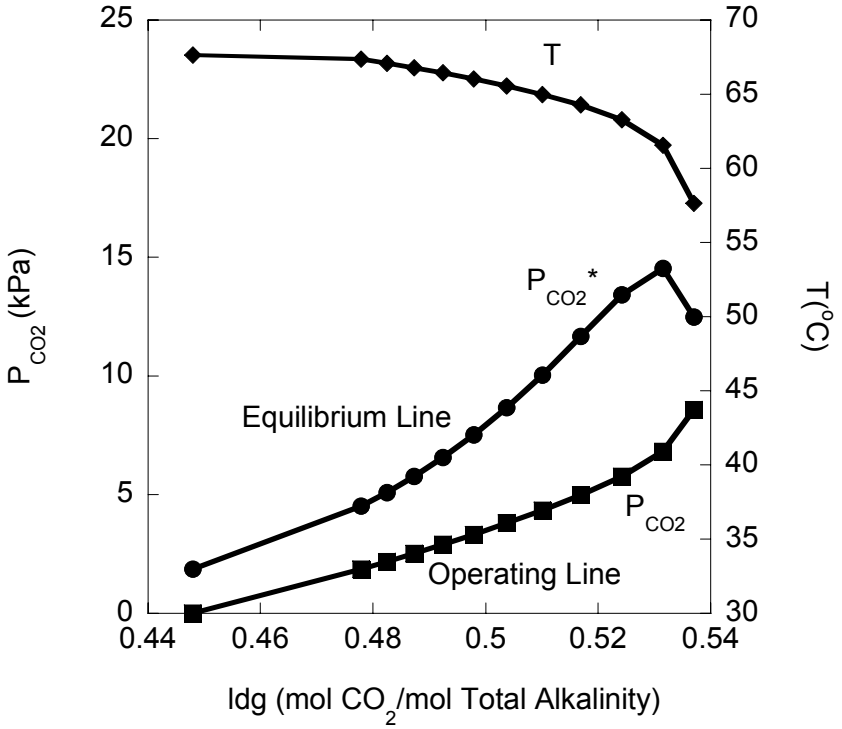

Figure 2. McCabe-Thiele Plot for 5m K^+/2.5m PZ, Vacuum Stripper at 30 kPa (Rich Loading = 0.537, Lean Loading = 0.448, T_{app} = 10°C

Conclusions and Future Work

In this quarter, equilibrium ACM models were developed for four configurations (matrix, split product, internal exchange and flashing feed). Our results show that the flashing feed gives the least equivalent work. It gives a 6% energy savings over the vacuum case. A rate-based model has been developed in ACM. The total equivalent work of stripping decreases with increasing stripper operating pressure for fixed liquid rate (30 gallons per minute), rich and lean loading and packing volume. Flashing of the rich feed and a rich end pinch is observed in the simple stripper (160 kPa). At 30 kPa, the mass transfer process is 95 % liquid film controlled. At 160 kPa the process is 81% and 70% liquid film controlled at the rich and lean ends.

In the next quarter, the rate-based model will be extended to structured packing and to other solvents. The pilot plant campaign results will be revisited in order to interpret the results which will help in the fine-tuning of the model.

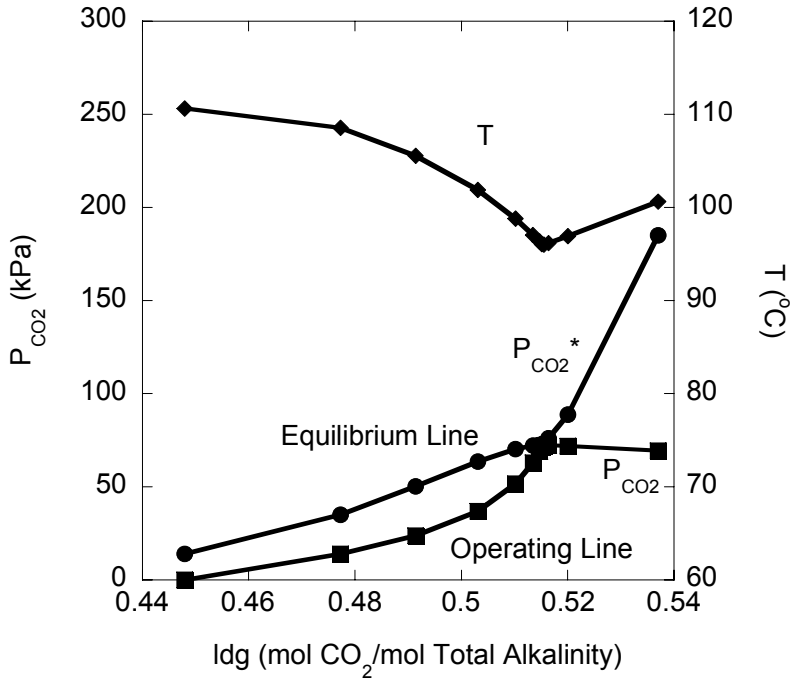

Figure 3. McCabe-Thiele Plot for 5m K^+/2.5m PZ, Simple Stripper at 160 kPa (Rich Loading = 0.537, Lean Loading = 0.448, T_{app} = 10°C

Task 2 – Pilot Plant Testing

Subtask 2.6 – Campaign 4

by Eric Chen

(Supported by EPA STAR Fellowship)

Introduction

In this reporting period, the final pilot plant campaign using potassium carbonate and piperazine was completed. Campaign 4 commenced at the beginning of January and was completed in early February. A total of 59 runs were completed. Approximately 300 liquid samples were taken and analyzed for CO_2 loading, piperazine and potassium concentration. The newly installed cross-exchanger reduced the approach temperature to less than 10°C.

Experimental

The pilot plant was operated for 12 days on a 24 hour basis for a total of 59 runs. The experiments were conducted with two different solvent compositions: 5m K^+/2.5m PZ and 6.4m K^+/1.6m PZ. The absorber and stripper were both packed with a new structured packing, Flexipac AQ Style 20, donated by Koch-Glitsch Inc. Each column contained 20 feet of packing, divided into 2 ten foot beds, with a chimney tray and redistributor in between each bed. The packing has a specific area of 300 m^2/m^3. The new packing has approximately 25% less area than Flexipac 1Y, the structured packing used in campaigns 1 and 2 and is design for high gas and liquid flow rates. In this campaign, the air cooler was in full operation and was used to protect the Vaisala CO_2 analyzers that were downstream. The newly installed cross-exchanger performed as designed and the trim heater and cooler were not used during the campaign (Figure 4). A summary of the absorber and stripper operations is shown in Table 7 and Table 8, respectively.

The liquid sampling procedure followed the standard methods developed over the course the last 3 campaigns. Ten mL of sample were withdrawn from the sample bombs with a syringe and then injected into a vial that contained 30 mL of de-ionized water (DI). For CO_2 loading analysis, the samples were further diluted by a factor of 40 and then analyzed on the Shimadzu 5050 Total Organic Carbon analyzer by utilizing its inorganic carbon analysis feature. 100ppm sodium carbonate/bicarbonate standards were placed every 6-7 samples to maintain quality control. The ion chromatography samples for the potassium and piperazine analyses were further diluted by a factor of 2000. The ion chromatograph was calibrated with standards that contained both piperazine and potassium.

Pilot Plant Operation

The liquid flow rates for the absorber middle and stripper middle sample points were extremely low, which made it difficult to fill the sample bombs. Since the bombs were made completely out of stainless steel, the sampler could not determine whether sufficient sample was taken. Therefore, a portion of the sample bombs were replaced with 1/2-inch PFA tubing. This allowed the sample taker to verify the integrity of the sample and greatly expedited the liquid sampling process.

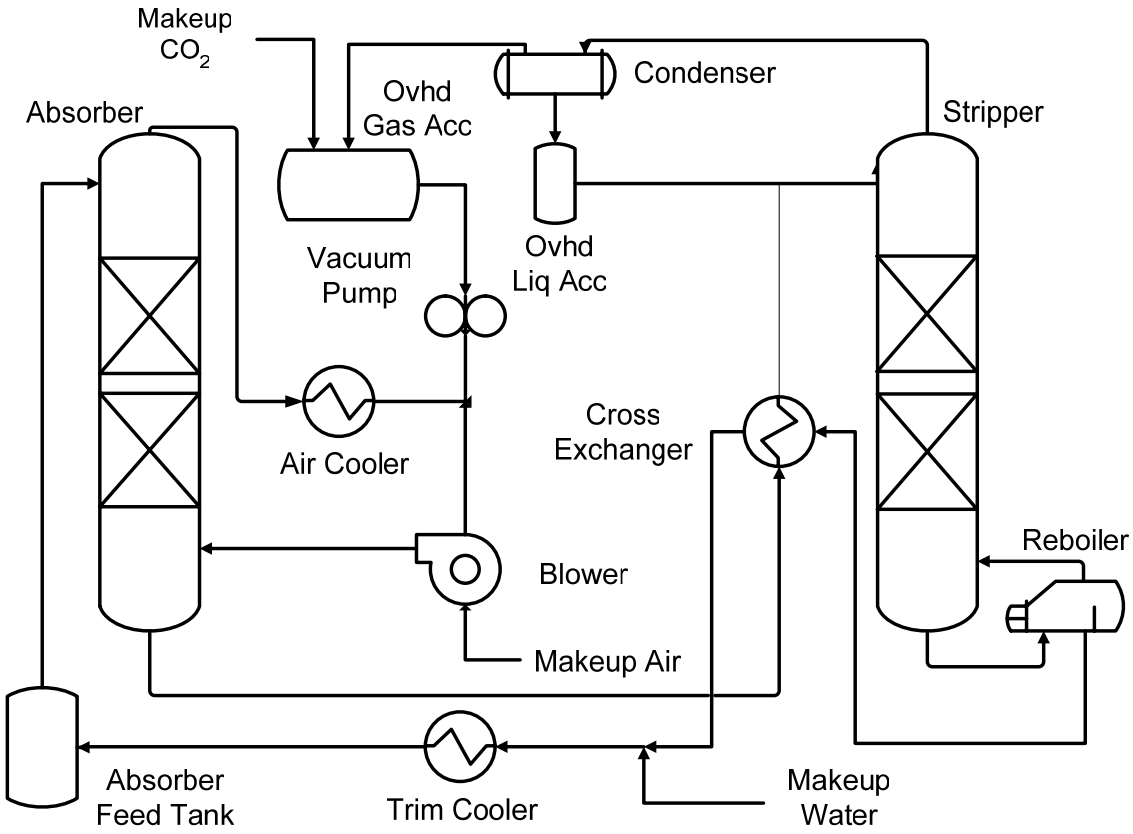

Figure 4. Campaign 3 Pilot Plant Flowsheet

Table 7. Absorber Operation

	5m K^+/2.5m PZ	6.4m K^+/1.6m PZ
Inlet CO_2 (mol %)	7.3 – 12.3	9.9 – 12.9
PZ Concentration (mol/kg solv)	1.4 – 1.5	1.0 – 1.2
K^+/PZ Ratio	2.1 – 2.3	3.9 – 4.0
Lean Ldg (mol CO_2/(K+2PZ))	0.39 – 0.45	0.45 – 0.51
G (kg/m^2-s)	1.2 – 2.0	1.2 – 2.0
L/G (kg/kg)	3.9 – 10.8	8.3 – 14.5
$T_{Gas,IN}$ (°C)	40	40 – 41
T_{LEAN} (°C)	40 – 46	39 – 46

Table 8. Stripper Operation

	5m K^+/2.5m PZ	6.4m K^+/1.6m PZ
ΔT Approach (°C)	6.9 – 8.9	3.7 – 6.4
Top Temperature (°C)	103 – 115	71.5 – 94
Bottom Temperature (°C)	117 – 118	77 – 97
Reboiler Heat Duty (kcal/mol CO_2)	85 – 290	90 – 180
NTU per pass (5 pass PFE)	1.5 – 2.1	1.5 – 1.9
$C_{P,COLD}/C_{P,HOT}$	1.04 – 1.08	1.05 – 1.11

In campaign 3, foaming was also observed. However, this time foaming was observed in the stripper instead of the absorber as in the first 2 campaigns. The temperature bulge was not as significant in the absorber and with the installation of the regenerative heat-exchanger; the temperature profile across the stripper was higher. Therefore, foaming it can be concluded that foaming may have some sort of temperature dependence. 800 mL of silicone based anti-foam was added throughout the duration of the campaign.

A carbon filter was installed in this campaign in an attempt to rectify the foaming the issues encountered in the first 2 campaigns. However, it was uncertain whether the carbon filter performed its intended function. The orifice plate that was installed in series with the carbon filter was sized improperly. The flow rate through the carbon filter was not measurable on the rotameter and hence, did not meet the design flow rate of 10-20% of the total liquid flow through the system.

Due to the lack of temperature control on the inlet absorber gas, a steam injector was installed. Steam was generated in a 6-inch reboiler using the distillate from the stripper and injected into the inlet gas to maintain a constant temperature of 40°C. The steam generator worked well for most of the campaign. However, in the middle of the campaign, the generator plugged up due to the accumulation of solids from the distillate. Apparently the distillate contained small amounts of potassium and carbonate and piperazine. Since the reboiler was never bled, solids accumulated over time and eventually impeded steam production. The 6-inch reboiler was bled, washed, and restarted. The reboiler operated without additional problems after the initial shutdown.

There were some solubility issues during the second half of the campaign after the composition was changed. The experiments with the 6.4m K^+/1.6m PZ solvent were designed to operate at the solubility limits of the solvent. As a result, any loss of water inventory in the system would cause solids to precipitate out. During the course of the operation, water was continually lost and at first could not be found. It was later discovered that water had begun to accumulate in the overhead CO_2 gas accumulator. Therefore, water had to be periodically pumped from the gas accumulator and back into the solvent stream, which resulted in some density fluctuations.

Before the start of this campaign, the pH meters were repaired and the transmitters were shielded from possible water intrusion with a makeshift cover. Both pH meters did not fail as in

the previous campaigns and perform quite well. Continuous online measurements were taken at the lean and rich end of the absorber. However, there were issues with maintaining a constant lean loading. It was concluded that having an additional pH meter upstream of the absorber feed tank would have facilitated this because it would give the operator direct feedback on the lean loading going into the feed tank. Then, adjustments to the heat duty could be made immediately instead of waiting for the residence time of the feed tank and finding out that the loading was incorrect or had drifted.

Results

The gas and liquid material balance calculated by the method used in campaign 2. However, in campaign 3, a third material balance was introduced. The CO_2 gas flow from the stripper recycle was measured with an annubar. The stripper gas capacity was determined by dividing the measured gas flow with the liquid flow rate. Figure 5 and Figure 6 show the material balance for the 5m K^+/2.5m PZ and 6.4m K^+/1.6m PZ solvent compositions. For some unknown reason, the material balance for the 6.4m K^+/1.6m PZ runs didn't close as well.

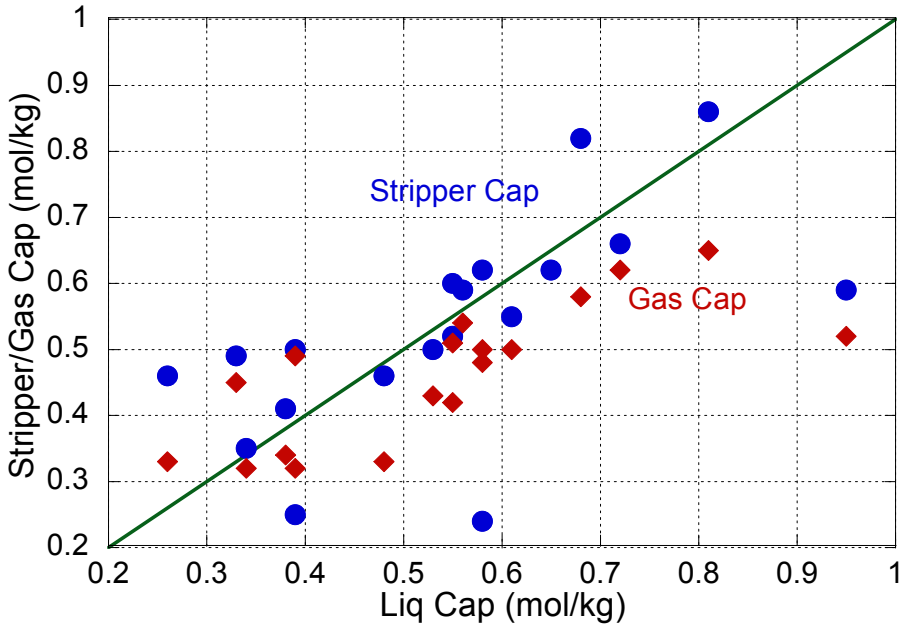

Figure 5. Mass Balance for 5m K^+/2.5m PZ

For the majority of the runs, the temperature bulge in the absorber was not as prominent as in the first and second campaigns due to the lower packing area. Figure 7 shows the temperature profile for the 5m K^+/2.5m PZ solution over a range of L/G ratios. For the 6.4m K^+/1.6m PZ solvent, at the same L/G ratio of 4 kg/kg, the temperature bulge is much smaller in magnitude due to the lower CO_2 absorption rate inherent to the solvent. Figure 8 shows the pH range and the corresponding lean and rich loadings that the absorber was operated. The pH measurements were corrected to a temperature of 40°C.

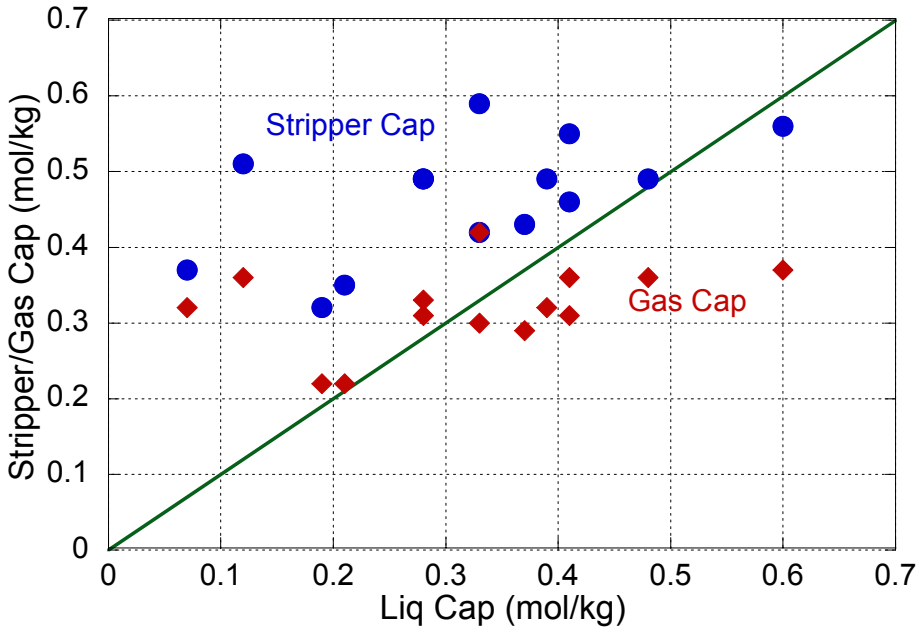

Figure 6. Mass Balance for 6.4m K^+/1.6m PZ

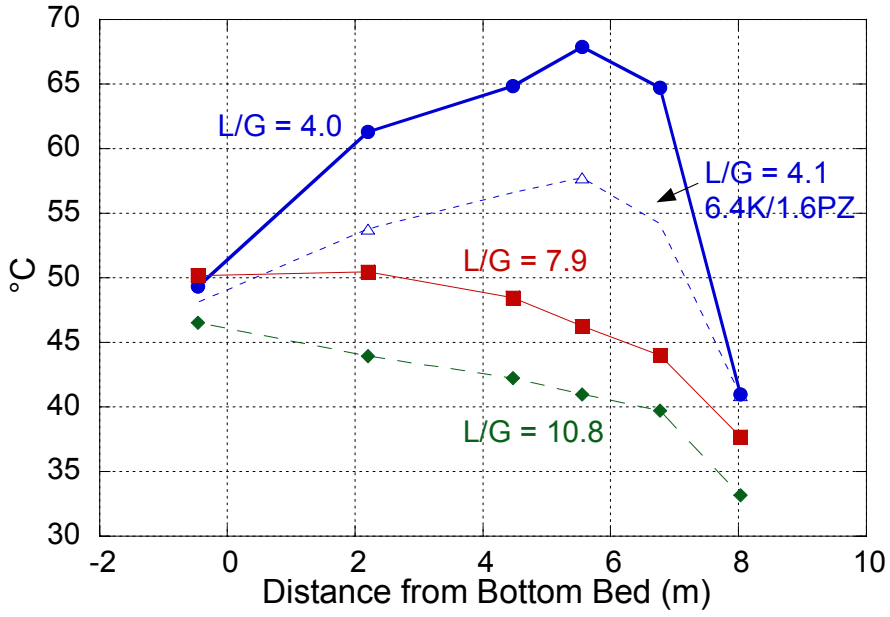

Figure 7. Absorber Temperature Profile

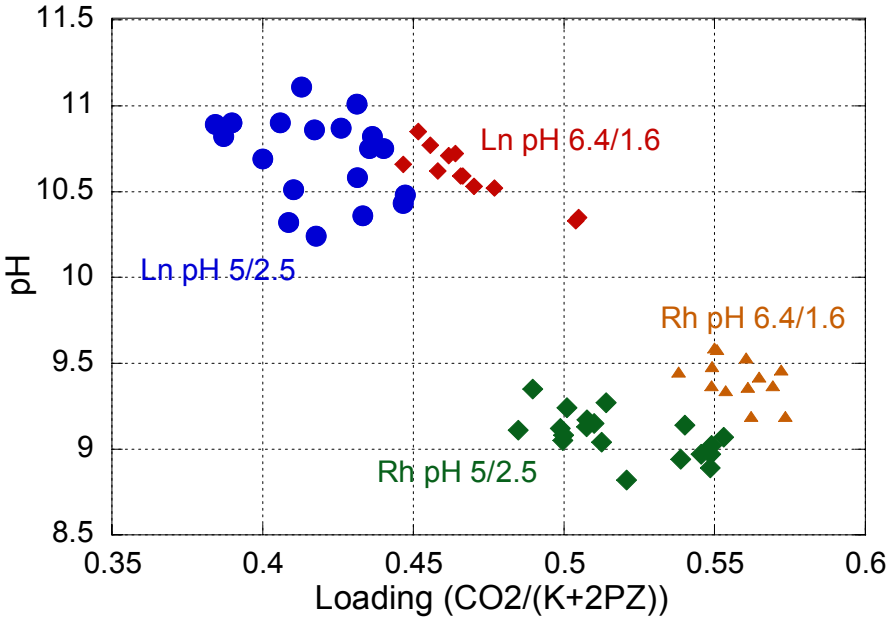

Figure 8. Absorber Loading Ranges

Figure 9 shows that reboiler heat duty increases with CO_2 removal efficiency for both the 5m K^+/2.5m PZ and 6.4m K^+/1.6m PZ solvent compositions. However, it appears that 5m K^+/2.5m PZ has a lower heat duty for a given CO_2 removal efficiency. The number of transfer units (NTU) per pass for the plate and frame cross-exchanger was calculated and plotted against the solvent flow rate. Figure 10 shows that the NTU's per pass are inversely related to the liquid flow rate. The approach temperatures of the 5m K^+/2.5m PZ and the 6.4m K^+/1.6m PZ solvent ranged from 6.9 to 8.9°C and 3.4 to 6.4°C, respectively. The approach temperature was lower for the 6.4m K^+/1.6m PZ because it was operated under vacuum and the stripper temperature profile was much lower. As a result, the NTU dependence is slightly different than the 5m K^+/2.5m PZ solvent.

Conclusions and Future Work

Campaign 4 was completed in early February and all of the liquid samples have been analyzed for CO_2 loading, piperazine, and potassium concentration. The newly installed plate and frame cross-exchanger worked very efficiently, achieving approach temperatures less than 10°C. Preliminary results show that the 5m K^+/2.5m PZ solvent had a lower heat duty as a function of CO_2 removal efficiency than the 6.4m K^+/1.6m PZ solvent.

The material balance for the gas phase needs to be resolved. Also the material balance for the 6.4m K^+/1.6m PZ solvent needs to be reconciled. Once, the material balances have been rectified, K_G calculations will be made to quantify and compare the CO_2 absorption performances of the two solvents.

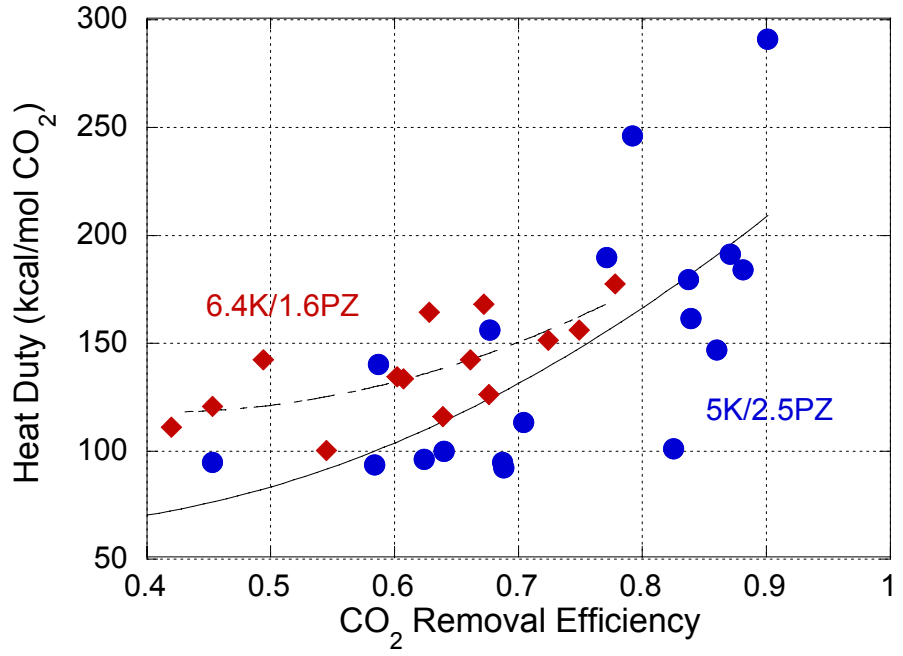

Figure 9. Stripper Performance

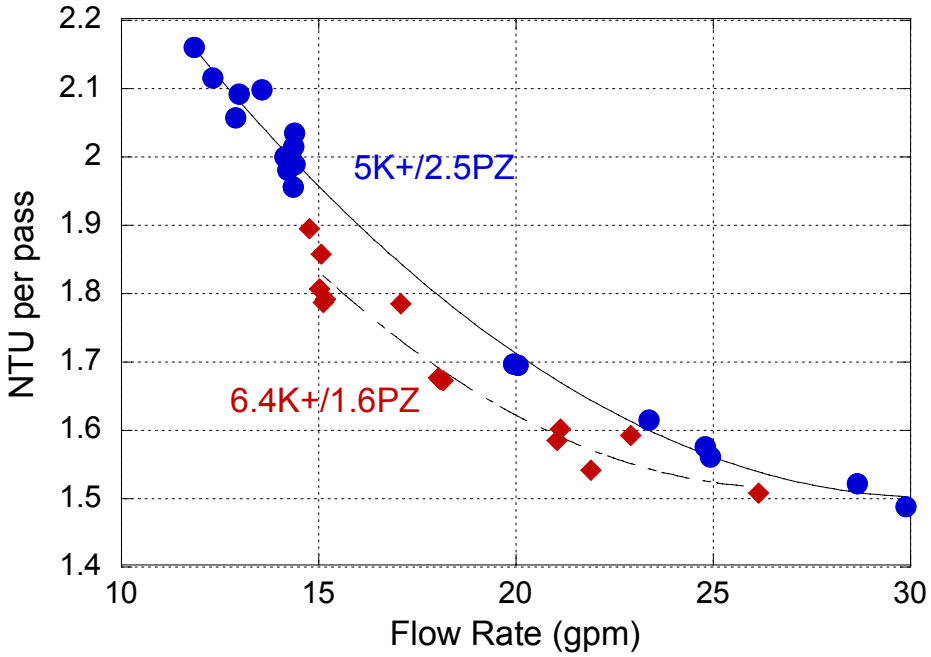

Figure 10. Plate and Frame Cross-exchanger Performance

Task 3 – Solvent Losses

Subtask 3.1 – Analysis of Degradation Products

Andrew Sexton

(Supported by the Industrial Associates Program in CO_2 Capture)

Introduction

This effort is an extension of work by Goff on the oxidative degradation of MEA. Goff showed that oxidative degradation can be mass-transfer limited by the physical absorption of O_2 into the amine and not by reaction kinetics. Goff also theorized that the oxidative degradation of MEA produced volatile ammonia as well as a host of other proposed degradation products. The major degradation products among these include formic acid, acetic acid, oxalic acid and glycolic acid. The oxygen stoichiometry necessary to produce these degradation products varies for each individual component; overall, it varies anywhere from 0.5 to 2.5 (Goff, 2004). Goff's work on MEA degradation was limited to analyzing MEA degradation rates via the evolution of NH_3. The ammonia evolution rates were measured using a Fourier Transform Infrared (FT-IR) analyzer.

This effort will extend Goff's gas-phase analysis by applying various methods of liquid-phase analysis, specifically ion chromatography and nuclear magnetic resonance. These analytical methods will be used to quantify the rate of amine degradation as well as the rate of degradation product formation.

The oxidative degradation of the amines may significantly affect the economics and environmental impact of these solvent systems. Oxidative degradation results in fragmentation of the amine solvent. The identity and quantity of degradation products is required to assess their impact on the environment and the process economics and to design for corrosion prevention and solvent reclaiming.

Experimental

As stated in previous quarterly reports, ion chromatography is the most extensively used liquid-phase analytical method. Anion chromatography utilizes a recently purchased AS15 (a low-capacity column designed to separate low-molecular weight anions, specifically acetate, glycolate, and formate) IonPac column made by Dionex. The column operates as a miniature adsorption tower. An unknown solution is injected into the column. An eluent of sodium hydroxide is continuously passed through the column to flush anions off the column and replenish it with hydroxide ions.

The ions leave the column and then pass through a suppressor, which provides a steady supply of H^+ ions. As a result, all other cations are flushed out of the system as waste, leaving a weakly ionized solution of H^+ ions and the unknown anion(s) in water. This solution is passed through a conductivity meter, which provides a signal peak with a specific height and area dependent upon the concentration of the anion in solution (Wang, 2005).

The most recent anion chromatography method analysis employs a linear gradient. The NaOH eluent starts at an initial concentration of 10 mM from time zero to eleven minutes. The weakly concentrated eluent is necessary to separate the low-molecular weight carboxylic acids, which tend to elute closely together. Once the low-MW compounds have eluted off the column, the method employs a linear gradient increasing from 10 to 45 mM NaOH from time eleven minutes to nineteen minutes. The eluent gradient stays constant at 45 mM until time thirty minutes; the concentrated assists in eluting the more strongly retained anions from the column. Lastly, there is a step change back to the original eluent concentration of 10 mM to allow the system to re-equilibrate prior to injection of the next sample. The eluent flowrate stays constant at 1.60 mL/min, and the columns are operated at 30 ^{o}C.

The cation chromatograph, located in the CPE building, operates in a similar manner. It utilizes a CS17 IonPac column manufactured by Dionex; it is a packed column containing a divinylbenzene/ethylvinylbenzene resin that separates cations based on their affinity for the resin. The eluent is methanesulfonic acid, or MSA (CH_3SO_3H), and the suppressor produces a steady supply of OH^- ions to flush out all other anions as waste. The end result is a weakly ionized solution of the unknown cation(s) and OH^- ions in water (Dionex, 2005). The anion IC is being used to quantify rates of degradation product formation (organic acids, nitrites, and nitrates), while the cation IC is primarily for characterizing the rate of amine degradation.

The method designed for degradation product analysis via cation chromatography uses a constant concentration of 13.5 mM MSA for thirty minutes. The eluent flowrate is 0.40 mL/min, and the columns are operated at 40 ^{o}C. When analyzing for amine concentrations, the concentration and flowrate are increased to 20 mM and 1.20 mL/min, respectively, for five minutes.

Nuclear magnetic resonance, or NMR, identifies unique ^{1}H atoms and/or ^{13}C atoms based on structure (double/triple bonds, attachment to acid/amine/etc. groups). Sealed liquid samples are subjected to a magnetic pulse, and each unique atom is characterized by a "chemical shift" on the readout. If the structure(s) in the solution is unknown, it may be necessary to construct a 2-D carbon-hydrogen correlation in order to determine structure. Samples must be prepared with approximately 10% D_2O (by weight) and DSS (Shoulders, 2005). D_2O, or deuterium oxide, is heavier than water and enhances the signal, thereby making the analysis easier. DSS, or Sodium 2,2-Dimethyl-2-Silapentane-5-Sulfonate, is used as a reference peak for aqueous solutions containing organic materials.

Results

Using the new analytical methods for the AS15 and CS17 columns, the following degradation experiments were analyzed for degradation product formation rates:

1. December 2004 MEA experiment (Oxidative degradation of 7 m MEA, 55^{o}C, 1400 RPM, 0.2 mM Cu, 0.4 moles CO_2/mol MEA, 98%O_2/2%CO_2).

2. September 2005 MEA experiment (Oxidative degradation of 7 m MEA, 55^{o}C, 1400 RPM, 0.2 mM Cu, 0.2 mM Fe, 0.4 moles CO_2/mol MEA, 98%O_2/2%CO_2).

3. November 2005 PZ experiment (Oxidative degradation of 2.5 m piperazine, 55°C, 1400 RPM, 350 ppm V^+, 98%O_2/2%CO_2).

4. January 2006 MEA experiment (Oxidative degradation of 7 m MEA, 55°C, 1400 RPM, 0.2 mM Cu, 0.2 mM Fe, 100 mM inhibitor A, 0.4 moles CO_2/mol MEA, 98%O_2/2%CO_2).

Also, two experiments were performed during the quarter, but haven't been analyzed:

1. March 2006 MEA experiment (Oxidative degradation of 7 m MEA, 55°C, 1400 RPM, 0.2 mM Fe, 0.4 moles CO_2/mol MEA, 98%O_2/2%CO_2).

2. March 2006 PZ experiment (Oxidative degradation of 2.5 m piperazine/5 m $KHCO_3$, 55°C, 1400 RPM, 500 ppm V^+, 98%O_2/2%CO_2).

The amine solutions were oxidized for 12 to 14 days in a jacketed reactor with low gas flow at 55°C. The solutions were agitated at 1400 RPM to produce a high level of gas/liquid mass transfer by vortexing. 98% O_2/2% CO_2 at 100 ml/min is introduced across the vortexed surface of 350 ml of aqueous amine. Samples were taken at regular intervals in order to determine how degradation products over the course of the experiment.

Figure 11 illustrates the concentration of significant degradation products from the oxidative degradation of piperazine, as determined by anion chromatography, over a 12-day experiment in the low gas flow degradation apparatus. Samples were taken at five intervals during the course of the experiment. Anion chromatography rates were determined last November; via cation chromatography, ethylenediamine has also been identified as a significant cationic degradation product. The most significant degradation products are formate and ethylenediamine. Towards the end of the experiment, it appears something happened within the reactor to significantly enhance mass transfer rates. Vigorous foaming began to occur, and the solution turned from a pale yellow to a very dark brown. Therefore, rates were calculated over the linear portion of the degradation curves.

In addition to the ethylenediamine, two other unknown cationic degradation products were observed from the piperazine experiment (in the analysis of degraded MEA samples, no cationic degradation products were observed). It is believed that these two products are most likely monoethanolamine, ammonium, or ethylamine. Figure 12 shows a plot of the area of the peaks of these two unknown degradation products, along with the observed area of EDA, versus experiment time. This figure shows that EDA is the most significant cationic product; the area of the two unknowns combined is approximately half the area of EDA.

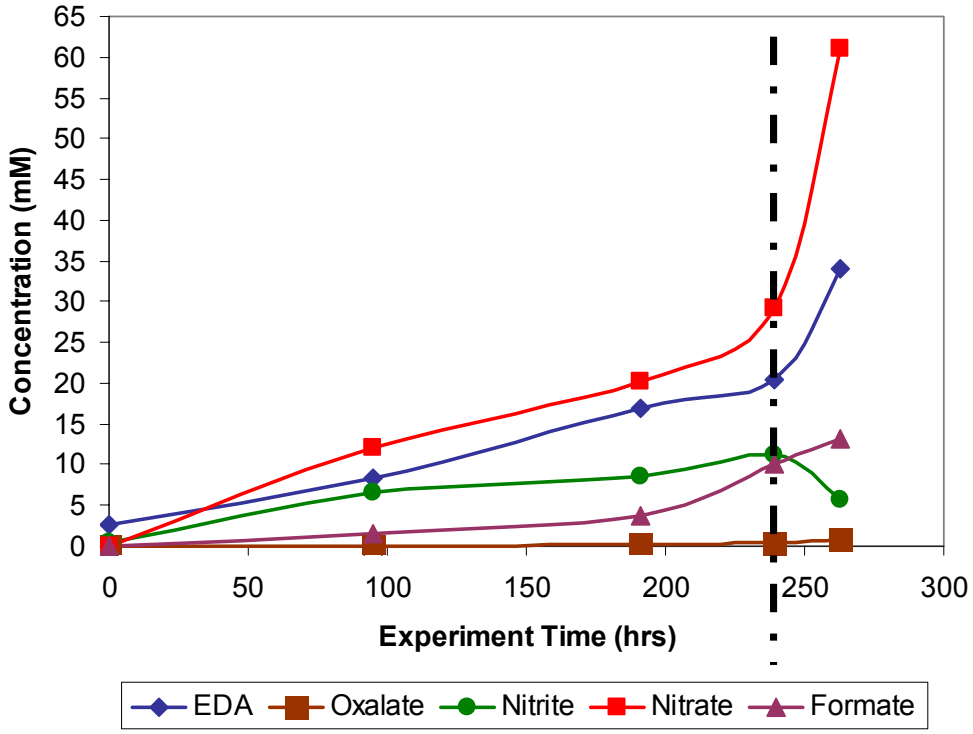

Figure 11 Oxidative degradation of 2.5 m Pz, 55°C, 1400 RPM, 500 ppm V^{+}

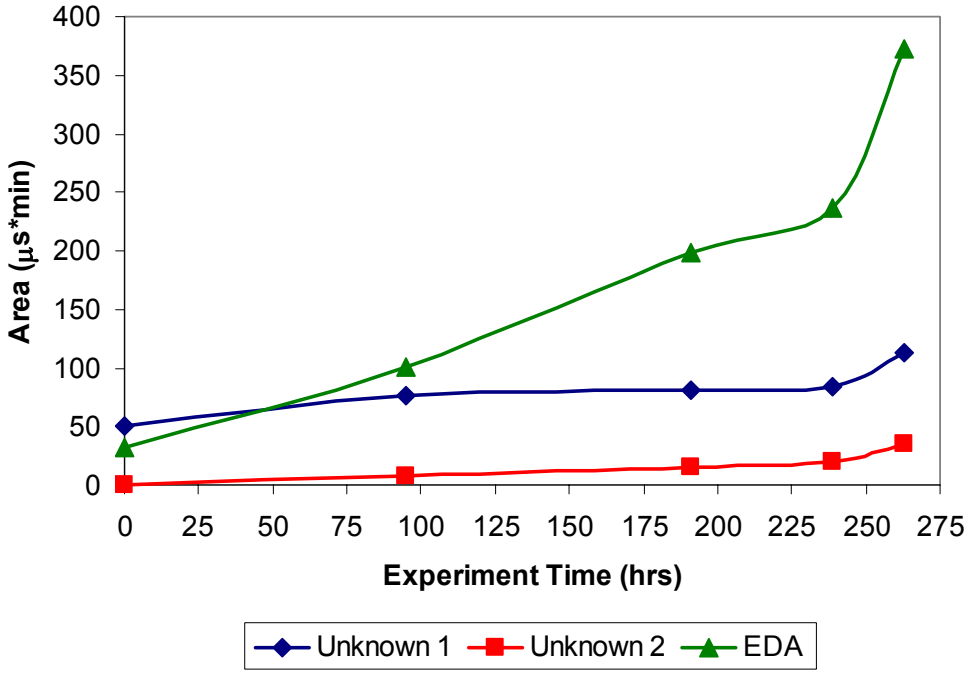

Figure 12 Oxidative degradation of 2.5 m Pz, 55°C, 1400 RPM, 500 ppm V^{+}

Figures 11 and 13 show the concentration of degradation products as a function of experiment time. Figure 13 refers to an experimentally degraded solution of 7 molal (mol MEA/kg solvent) MEA with 0.2 mM copper present; figure 12 depicts the oxidative degradation of 2.5 molal piperazine solution with 500 parts per million (ppm) of vanadium added. Vanadium is used in piperazine solutions as a corrosion inhibitor; similarly to copper, it's also believed to be a degradation inhibitor. Both of these experiments were carried out for approximately twelve days; analysis was performed November 2005 using anion chromatography.

According to the ion chromatography analysis, acetate/glycolate and formate are the most abundant degradation products. Acetate/glycolate is combined because when these samples were run, the peaks for these compounds were co-eluting under the same peak. Nitrite, nitrate, and oxalate have been identified as minor products. At the final time of 12 days, acetate/glycolate, formate, nitrite, nitrate and oxalate are present at concentrations of 156, 133, 38, 20 and 15 millimolar, respectively. This corresponds to degradation rates of 0.54, 0.46, 0.13, 0.08 and 0.05 mM/hr.

The degraded piperazine solution was analyzed using anion and cation chromatography. Formate, oxalate, nitrite and nitrate were identified as anionic degradation products; ethylenediamine is the lone identified cationic degradation product. Nitrate (0.13 mM/hr) and ethylenediamine (0.09 mM/hr) are the most abundant degradation products; nitrite, oxalate, and formate are also present. In March 2006, these experiments were re-analyzed using the most recently developed analytical method using the AS15. The results are shown in Figures 14 and 15.

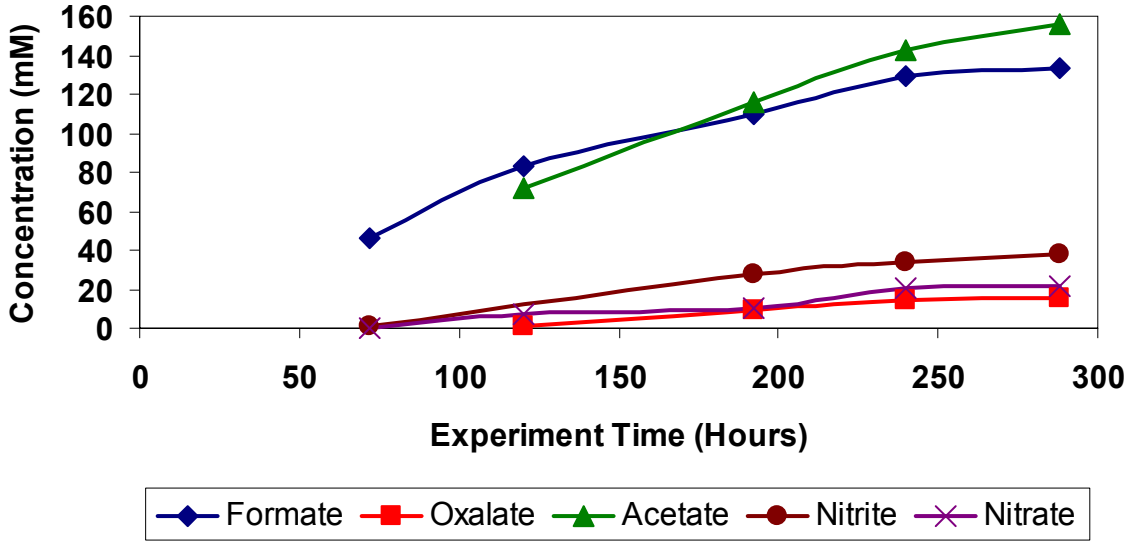

Figure 13 Oxidative degradation of 7 m MEA, 0.2 mM Cu, 55°C, 1500 RPM

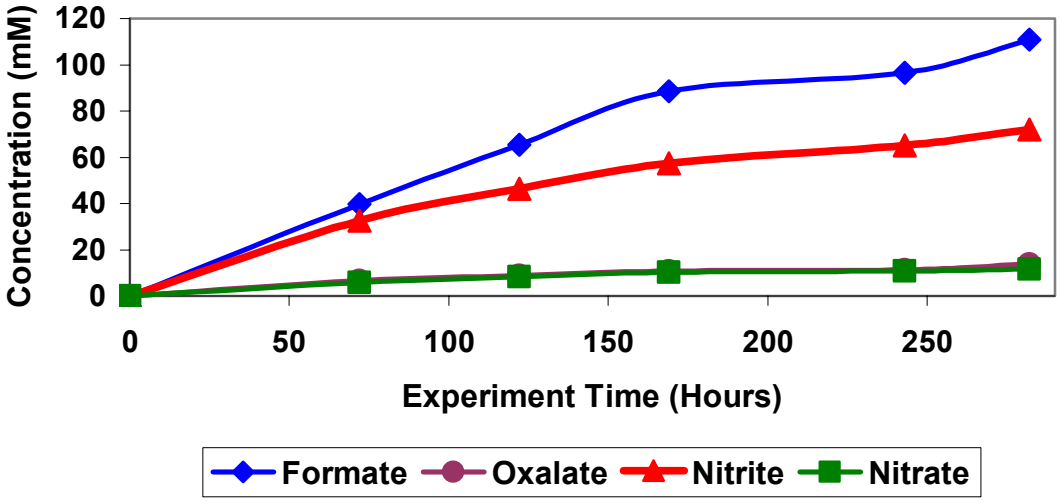

Figure 14 Oxidative degradation of 7 m MEA, 0.2 mM Cu, 55°C, 1500 RPM

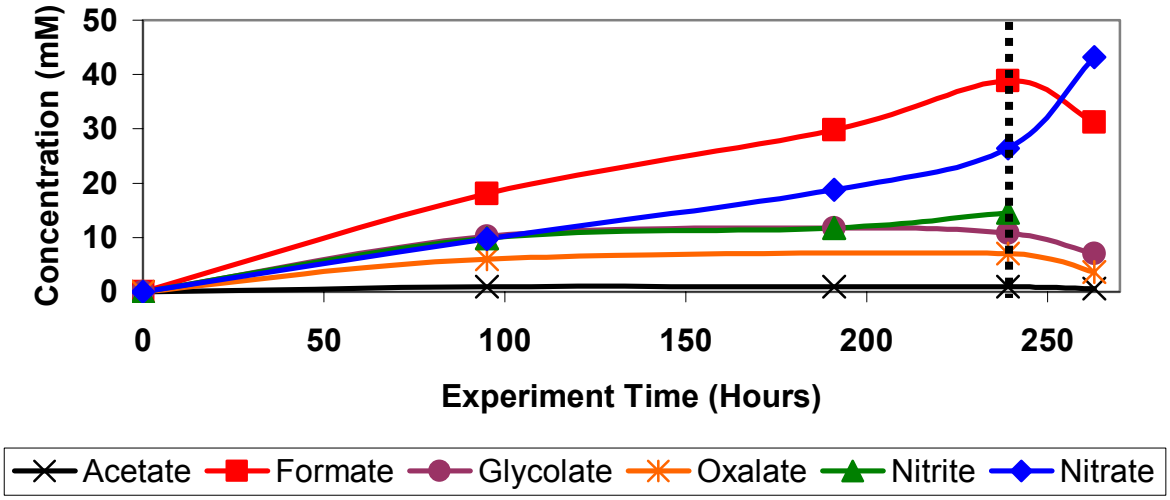

Figure 15 Oxidative degradation of 2.5 m Pz, 55°C, 1400 RPM, 500 ppm V^{+}

Figure 16 depicts the production of degradation products when 7 molal MEA is degraded in the presence of 0.2 mM of iron and copper, along with the addition of 100 mM of inhibitor A. All four carboxylic acids were detected along with nitrate and nitrite, albeit in much smaller quantities than in the other degradation experiments.

Tables 9 and 10 summarize degradation rates (in mM/hr) for all previously performed degradation experiments. In addition to the experiments depicted in prior figures, degradation products from the 9/05 MEA experiment (7 m MEA with 0.2 mM Cu and Fe added) and the three high gas flow degradation experiments have been quantified. Table 9 summarized analysis performed in March/April 2006; table 10 summarizes analysis from November 2005.

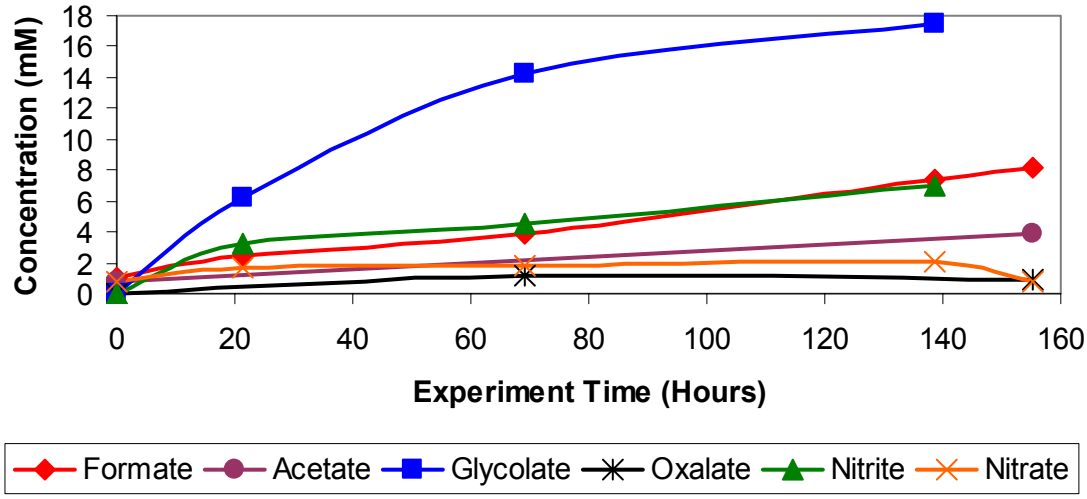

Figure 16 Oxidative degradation of 7 m MEA, 0.2 mM Cu/Fe, 100 mM A, 55°C, 1500 RPM

Cation chromatography work was also done for pilot plant solutions from the most recent piperazine campaign. Pilot plant samples were run to analyze for piperazine and potassium concentrations. Over the course of two weeks, the potassium to piperazine ratio increased from 2.17 to 2.27. For the first campaign, the ratio was approximately 2. Since the potassium concentration in the solution is supposed to remain constant, one can infer that the amount of piperazine in the pilot plant is decreasing as a result of degradation. Furthermore, the pilot plant samples were analyzed for any degradation products. All the samples contained 2 to 3 mM of EDA, as compared to approximately 20 mM in the experimentally degraded samples.

NMR analysis was performed on the experimentally degraded piperazine samples to confirm the presence of ethylenediamine. Figures 17 and 18 below confirm the presence of EDA in these solutions.

Table 9 Summary of Degradation Product Formation Rates in mM/hr – 11/05 Analysis

Experiment	12/2006	09/2006	01/2006	11/05 Pz	5/3/2005	5/9/2005	5/16/2005
Distinguishing Conditions	0.2 mM Cu	0.2 mM Cu and Fe	0.2 mM Cu and Fe, 100 mM "A"	500 ppm V+	α = 0.15, 4 mM Cu, 270 mM "A"	α = 0.15, 4 mM Cu, 0.2 mM Fe, 270 mM "A"	α = 0.40, 4 mM Cu, 0.2 mM Fe, 270 mM "A"
Acetate (mM/hr)	0.03	0.02	N/A	<0.01	0.18	0.14	0.40
Glycolate (mM/hr)	0.12	0.02	0.13	0.03	1.29	1.19	1.97
Formate (mM/hr)	0.39	0.63	0.05	0.12	4.40	7.99	2.13
Oxalate (mM/hr)	0.04	0.04	0.01	0.01	0.33	0.48	0.44
Nitrate (mM/hr)	0.06	0.13	0.01	0.16	0.15	0.11	0.02
Nitrite (mM/hr)	0.33	0.28	0.05	0.06	0.10	N/A	0.08
EDA (mM/hr)	N/A	N/A	N/A	0.09	N/A	N/A	N/A

Table 10 Summary of Degradation Product Formation Rates in mM/hr – 3/06 Analysis

Experiment	12/2006	09/2006	09/2006	11/05 Pz	5/3/2005	5/9/2005	5/16/2005
Distinguishing Conditions	0.2 mM Cu	0.2 mM Cu and Fe	0.2 mM Cu and Fe	500 ppm V+	α = 0.15, 4 mM Cu, 270 mM "A"	α = 0.15, 4 mM Cu, 0.2 mM Fe, 270 mM "A"	α = 0.40, 4 mM Cu, 0.2 mM Fe, 270 mM "A"
Acetate/Glycolate (mM/hr)	0.26	0.34	0.31	N/A	1.77	3.60	2.90
Formate (mM/hr)	0.33	0.64	1.11	0.05	2.34	4.67	6.67
Oxalate (mM/hr)	0.03	0.03	0.03	<0.01	0.86	0.86	1.04
Nitrate (mM/hr)	0.07	0.20	0.20	0.23	N/A	N/A	N/A
Nitrite (mM/hr)	0.18	0.26	0.27	0.02	N/A	N/A	N/A
EDA (mM/hr)	N/A	N/A	N/A	0.09	N/A	N/A	N/A

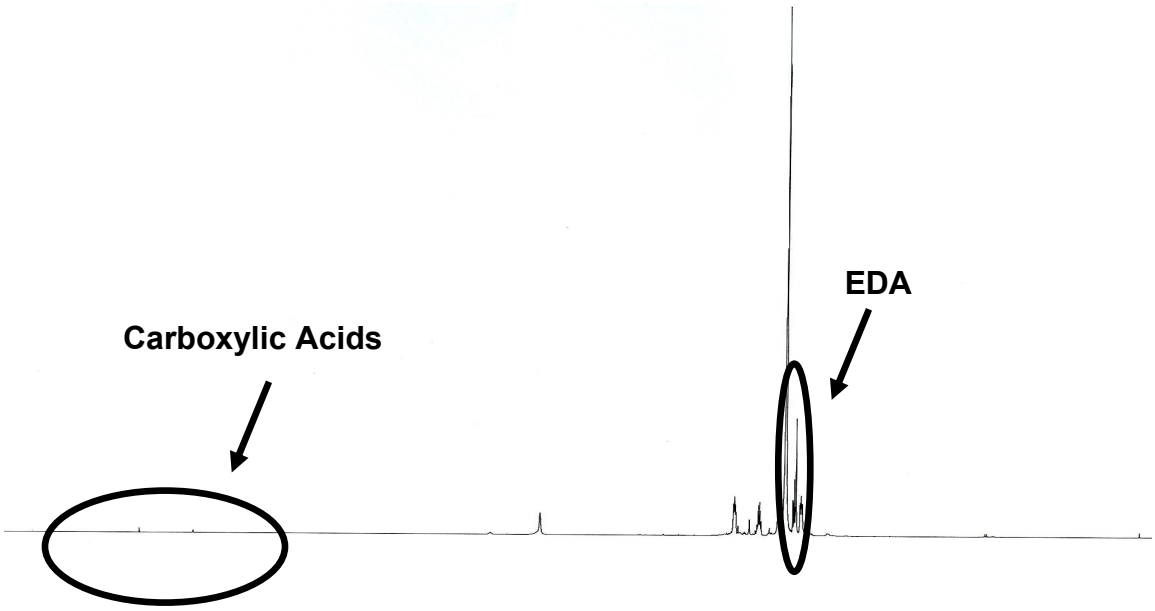

Figure 17 ^{1}H NMR analysis oxidatively degraded piperazine

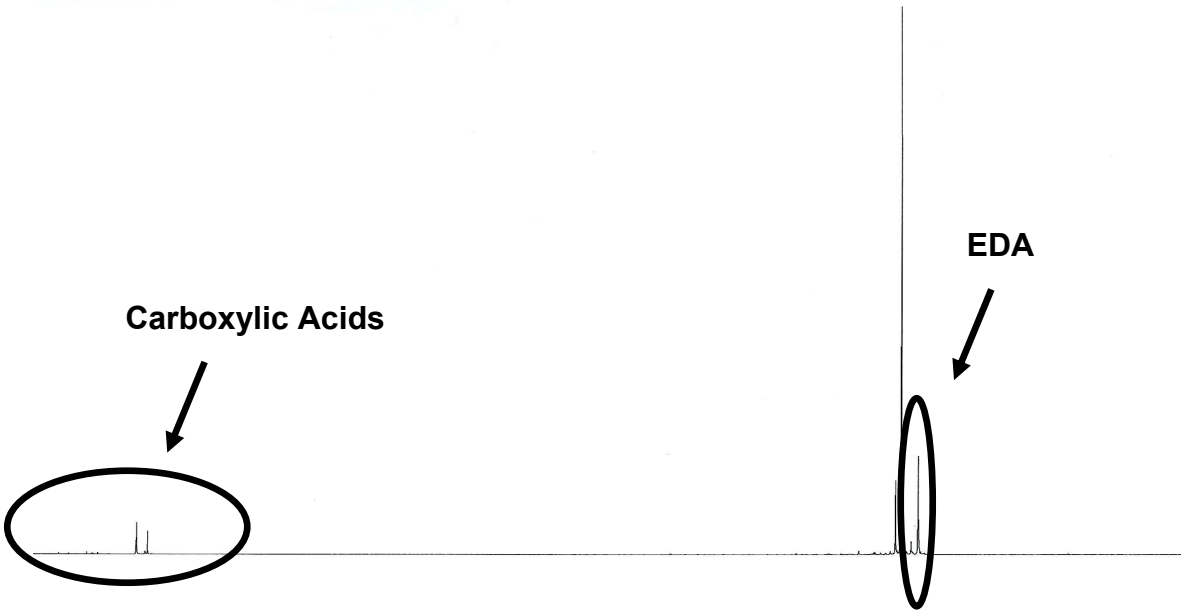

Figure 18 ^{13}C NMR analysis oxidatively degraded piperazine

Conclusions and Future Work

The four carboxylic acids have been identified as reaction products of amine degradation, confirming the finding in the Dow Rooney paper. In addition, nitrite, nitrate, and ethylenediamine have been discovered as significant amine degradation products. Based on the most recent ion chromatography analysis, formate and nitrite are the most abundant products of the oxidative degradation of monoethanolamine – when inhibitor A is not present. Calculated concentrations of products from the high gas flow degradation apparatus confirm that formate is more abundant than acetate and glycolate. However, nitrate and nitrite concentrations are very low in the high-gas flow degradation apparatus. This lends to the hypothesis that nitrate and nitrite are formed through an initial NO_x degradation product, which is stripped out in the high-gas flow apparatus.

Furthermore, data from the high gas flow experiments shows that a combination of copper and iron produce more formate than copper by itself; it also shows a shift in degradation product formation from a lower CO_2 loading to a higher CO_2 loading. The amount of acetate and glycolate relative to formate increases, and the overall degradation product formation rate decreases significantly. A similar trend is observed in the low gas flow degradation apparatus; more formate is produced when iron and copper are both present as opposed to just copper. Moreover, analysis suggests that chemistry shifts away from glycolate when copper is present. The presence of copper may also shift degradation production from nitrite and nitrate.

When inhibitor A is present in 7 m MEA in the presence of copper and iron, oxidative degradation is reduced greatly. Glycolate is the most prevalent degradation product when inhibitor A is present, but it's in a much smaller quantity than the most abundant product in other MEA experiments. From this analysis, one can conclude that inhibitor A does an excellent job at slowing down the rate of MEA degradation.

When inhibitor A is not present, the rate of piperazine oxidative degradation is much slower than the rate of MEA degradation. Ethylenediamine is a degradation product specific to piperazine. There is also a shift in the type of degradation products. When MEA is degraded, the carboxylic acid degradation products appear in greater quantities than nitrogen-containing products (nitrite, nitrate, and EDA). On the other hand when piperazine is degraded, the opposite is true. Further MEA and piperazine samples will be degraded and analyzed to confirm these conclusions.

There are still some issues to resolve regarding the IC analysis. Two anionic and two cationic degradation products remain unidentified. The two anionic species are interfering with the glycolate and acetate analysis. The method will need to be further modified to separate these peaks. Quantifying these degradation products and understanding oxidation chemistry will improve the environmental, process, and economic value of the CO_2 removal system.

Task 5 – Corrosion

By Amorvadee (Amy) Veawab

Associate Professor, University of Regina

Supported by subcontract

Research Objectives

The carbon dioxide (CO_2) absorption process using aqueous chemical solutions is subject to a number of operational difficulties, of which the most severe is corrosion of process equipment and solvent degradation. Corrosion problems have been receiving a great deal of attention because they have substantial impacts on the plant's economy, especially in terms of unplanned downtime, production losses, reduced equipment life, and extra-expenditure for restoring the corroded equipment and for treatment systems initiated to mitigate the corrosion. The corrosion problems also prevent the absorption process from achieving energy efficient operations.

The aqueous solution of blended potassium carbonate and piperazine has demonstrated to be a promising solvent for CO_2 capture from coal-fired power plant flue gas due to its capture performance and energy efficiency. It is our goal to further explore the promise of this solvent in an aspect of the potential operational problems. This project focuses on the investigation of corrosion of materials during CO_2 absorption and solvent regeneration in the presence and absence of solvent degradation products and chemical additives including oxidative inhibitors and corrosion inhibitors.

The research involves comprehensive literature review on the corrosion in CO_2 absorption process using potassium carbonate and piperazine, and experimental evaluations in the following sequences.

Task 1: Evaluation of corrosion in base solution (the blended potassium carbonate and piperazine) against the corrosion in an aqueous solution of monoethanolamine (MEA).

Task 2: Evaluation of corrosion in base solution containing degradation products.

Task 3: Evaluation of corrosion in base solution containing degradation products and oxidative inhibitors.

Task 4: Evaluation of inhibition performance of corrosion inhibitor in the presence of degradation products and oxidative inhibitors.

Progress

Dr. Veawab has led the implementation of this research with a great assistance from one graduate student, Ms. Manjula Nairnar. Ms. Nainar has enrolled in our Master program in September 2005. She has a strong background in electrochemistry, which is extremely useful for corrosion experiments and analysis.

Over the past four months, the following tasks were completed.

1) Assembly of a bench-scale electrochemical corrosion setup
2) Validation of electrochemical corrosion setup and experimental procedures

3) Benchmarking corrosion rate and behavior of carbon steel in an aqueous solution of 5 kmol/m^3 (molar) MEA

4) Benchmarking corrosion rate and behavior of carbon steel in an aqueous solution of 5 m. $KHCO_3$/ 2.5 m. piperazine

1) Assembly of a bench-scale electrochemical corrosion setup

1.1 Experimental setup

Figure 19 is a schematic diagram of experimental setup for electrochemical corrosion tests. The setup consists of a corrosion cell, a potentiostat, a water bath equipped with a temperature controller, a gas supply set, a condenser, a data acquisition system, a pH meter and a conductivity meter. The corrosion cell (Figure 20) is a standardized three-electrode cell approved by the ASTM (model K47 from EG&G instruments corporation, Princeton Applied Research, NJ, USA). It is a fully equipped glass vessel used for simulating corrosive environment. The K47 cell consists of:

1. A one-liter flask with a flat bottom to prevent tipping,
2. A leak proof assembly for mounting working electrode (test specimen) at the center of the cell. Its assembly includes stainless steel threaded rod, spacer, electrode holder, mounting rod and PTFE gasket.
3. Twin high-density, non-permeable counter or auxiliary electrodes,
4. A salt bridge connection,
5. A calomel reference electrode (SCE) ($Hg/HgCl_2$/ saturated KCl),
6. A gas inlet and outlet for transferring gas to and from the cell.

The potentiostat is an electronic device capable of supplying and controlling the potentials of working electrodes (specimen) and also measuring the currents produced from the corrosion cell. A model 273A potentiostat (EG& G Instruments Corporation, Princeton Applied Research, NJ, USA) providing an accuracy of $\pm$ 0.2% of the potential and current readings, was used. To ensure its performance, the 273A potentiostat was calibrated regularly by using a built in calibration function mode.

The water bath was equipped with a temperature controller to maintain a constant water temperature within $\pm$ 0.1^oC throughout the experiment. To minimize heat loss (or gain) to or from the surroundings, the water surface was covered with hollow balls. The gas supply set was a source of gases, carbon dioxide (CO_2) and nitrogen (N_2). These gases were introduced into the corrosion cell for simulating the test environment, through a series of gas flow meters that can measure the gas flow rate within $\pm$ 2% accuracy.

The Allihn condenser (jacket length of 300 mm and a height of 445 mm) was connected to the cell to prevent any change in solution concentrations due to evaporation.

The data acquisition system, model 352 SoftCorr III (EG& G Instruments Corporation, Princeton Applied Research, NJ, USA) was installed into a Pentium IBM compatible computer in order to control the potentiostat and also to record and analyze the produced corrosion data.

The pH meter, model pH 11 series (Oakton, USA) was used for measuring the pH value of the test solution with an accuracy of $\pm$ 0.01. The conductivity meter model YSI 3200 conductivity meter was used to measure the conductivity of the test solution with an accuracy of $\pm$ 0.10%. Both the meters were calibrated regularly with standard solutions.

1.2 Specimen preparation

Two types of specimens used in this work are stainless steel 430 (SS 430) and carbon steel 1018 (CS 1018). SS 430 was regularly used for standardizing the experimental procedures and instrumentation in electrochemical tests, whereas CS 1018 was used for all actual electrochemical tests. The specimens used for electrochemical experiments were cylindrical in shape with length, outside diameter, and hole diameter of 0.500 inch (1.270 cm), 0.375 inch (0.952 cm), and 0.210 inch (0.533 cm), respectively. Prior to experiments, the specimens were prepared by wet grinding with 600 grit silicon carbide papers using deionized water in accordance with the ASTM standard G1-90 (1999). They were then degreased with high purity methanol and dried with hot air.

1.3 Experimental procedure

- Prepare 1 liter of solution with desired concentrations and CO_2 loading.
- Transfer 900 mL of the prepared solution to a corrosion cell, and transfer the remaining solution to a salt bridge.
- Place the corrosion cell in a water bath to control the solution temperature at desired values (e.g. $80 \pm 0.10^{o}C$).
- Connect the corrosion cell to the condenser, and purge it with appropriate mixture of N_2 and CO_2 to maintain a desired CO_2 loading of solution. The N_2 gas was typically purged for 30 minutes to stabilize the cell's environment.
- Prepare the specimen to be tested by degreasing it with 99.90% methanol, and mount it on a specimen holder.
- Adjust the tip of salt bridge to be about 2 mm away from the specimen.
- Connect the corrosion cell to the potentiostat equipped with the data acquisition software, and specify types and settings of corrosion measuring technique in the software.
- Start the polarization scan when the potential of specimen reaches equilibrium, or is constant with time.
- Measure pH and conductivity of the solution before and after each experiment.
- Sample the solution before and after each experiment for titration to determine the solution concentration and CO_2 loading.
- Replicate the experiment to ensure data reproducibility.

1.4 Corrosion measuring techniques

(a) Tafel plot

Tafel plot is a widely used and accepted method for determining corrosion rate. This technique involves generating an anodic/ cathodic polarization curve of a specimen in the potential range of ± 200 mV from equilibrium corrosion potential (E_{corr}). A typical Tafel plot is illustrated in Figure 21. With anodic (β_a) and cathodic (β_c) Tafel slopes and corrosion current density (i_{corr}) obtained from the plot, corrosion rate can be calculated by using the following equation.

$$CR = \frac{\left(3.272 \times 10^{-3} \times i_{corr} \times E.W.\right)}{A \times D} \qquad (1)$$

where CR is corrosion rate in mmpy, i_{corr} in μA/cm^2, $E.W.$ is equivalent weight of specimen, A *is* area of working electrode in cm^2, and D is density of the specimen in g/cm^3.

(b) Potentiodynamic polarization

Figure 22 illustrates a typical potentiodynamic polarization curve of a specimen under a given environment. The curve consists of two branches, cathodic and anodic branches, representing reduction of oxidizing agent and oxidation of specimen, respectively. The cathodic curve is below the corrosion potential (E_{corr}) whereas the anodic is above. The anodic curve can be divided into three regions, namely active, passive, and transpassive. The active region is the region in which the current density increases rapidly with increasing potential from E_{corr} in the positive direction. The current density starts decreasing after reaching a particular potential, which indicates the initiation of film formation. The potential at which the film begins to form on the metal surface is called primary passivation potential (E_{pp}). The current density becomes constant at a particular potential, which indicates the completion of film formation (E_{cp}). Then the current density increases rapidly at a potential, which is called as transpassive potential (E_{trans}). The region between the primary passivation potential and transpassive potential is called passivation region, because the film formation generally retards the corrosion by forming a barrier between the metal and solution. The region beyond the transpassive potential where the corrosion rate increases rapidly is called transpassive region. This indicates that the film formed is broken and further corrosion and pits are formed on the metal surface.

(c) Cyclic polarization

Cyclic polarization is an extension of potentiodynamic polarization providing a supplementary capability in identifying the presence of pitting corrosion and the ability of the metal to repair after the pits occur. The cyclic polarization curve is essentially a combination of a forward scan of potentiodynamic polarization and a reverse scan towards the corrosion potential (E_{corr}) added to the forward scan (Figure 23). The cyclic polarization curve can be found in either negative or positive hysteresis. If the reverse scan shows a negative hysteresis compared to forward scan, pitting corrosion is unlikely to occur. On the contrary, if the reverse scan shows a positive hysteresis, pitting corrosion is likely to occur, pits tend to initiate, and any damage to the passive film cannot be self repaired. Furthermore, pits will continue to grow when the repassivation potential (E_{rp}) is greater than E_{corr}.

2) Validation of experimental setup and procedures

The experiments were validated accordingly to the ASTM standard G5-90 (1999). The anodic polarization was carried out using SS 430 specimen in 1N sulfuric acid (H_2SO_4) solution at 30 ^oC. The corrosion cell was purged with nitrogen at a flow rate of 150 cm^3/min for 30 minutes. The working electrode (SS 430 specimen) was prepared by wet polishing with 600 grit silicone carbide papers. The obtained polarization curves were then compared with the ASTM reference band generated from other laboratories that followed this standard procedure. Figure

24 demonstrates that the obtained curve falls within the reference band, thus validating the experimental instrumentation and procedures.

3) Benchmarking corrosion of carbon steel in aqueous MEA-CO_2 system

Figure 25 illustrates the cyclic polarization curve of carbon steel in the presence of 5 kmol/m^3 MEA containing a CO_2 loading of 0.20 mol/mol at 80 ^oC. This system manifests a typical active, passive, transpassive behavior of carbon steel. Under the test condition, the tested carbon steel specimen is clearly in an active state with no passive film formed on the surface, thus allowing a series of half-cell oxidation and reduction corrosion reactions to occur. This is evidenced by the increase in anodic current density with potential. As the potential raised beyond the primary passivation potential (E_{pp}), film starts passivating on the metal surface. As a result, the system corrosiveness reduced substantially, as indicated by decrease in current density. The passive film eventually broke down at E_{trans}. There is no tendency of pitting occurrence.

4) Benchmarking corrosion of carbon steel in aqueous $KHCO_3$ – piperazine system

Figure 25 also illustrates the cyclic polarization curve of carbon steel in the presence of an aqueous solution of 5 m. $KHCO_3$ – 2.5 m. piperazine at 80^oC. Similar to the MEA system, the $KHCO_3$-piparizine system manifests a typical active, passive, transpassive behavior of carbon steel. In the active region, it is apparent that the cathodic and anodic current densities of $KHCO_3$-piperazine system are greater than those of MEA system, indicating a higher corrosion rate in $KHCO_2$-piperazine system. This is evidenced by high conductivity values shown in Table 11. It should be noted that further investigation of pitting tendency is required since there are oscillations of current density during experiment in the passive of forward and backward potential scan.

Figure 26 illustrates the polarization curves of carbon steel in the presence of an aqueous solution of 5 m. $KHCO_3$ – 2.5 m. piperazine at various temperatures. It is apparent that solution temperature has a great impact on corrosion rate and behavior of this system. An increase in temperature shifts the polarization curves (both cathodic and anodic branches) in the positive direction. This is probably due to an increase in the concentrations of oxidizing agents and of Fe^{2+}, which gives an increase in the rate of both oxidation and reduction reactions.

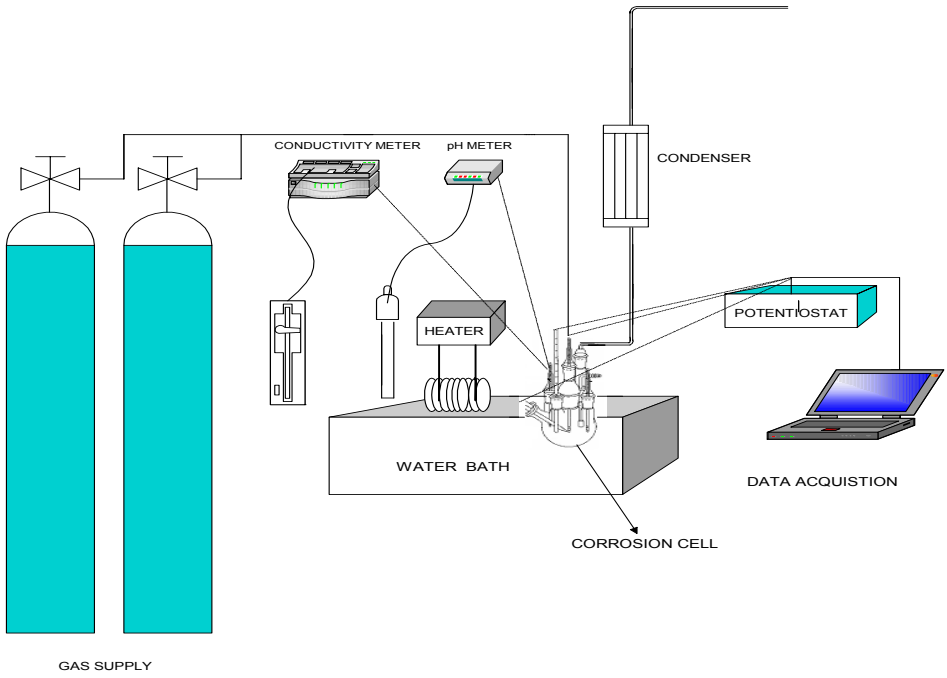

Figure 19: Experimental setup for electrochemical corrosion tests.

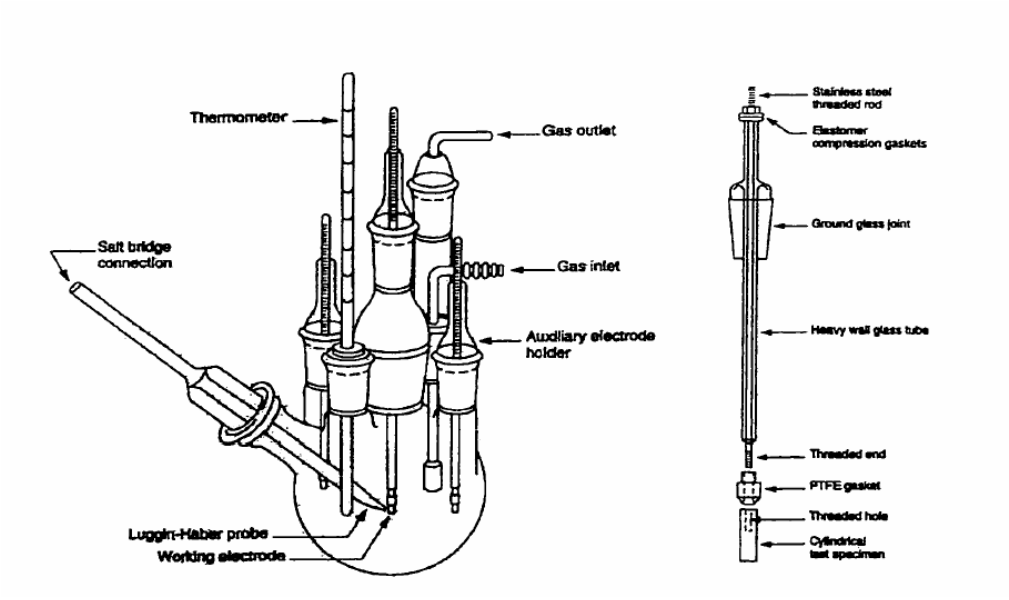

Figure 20: The ASTM corrosion cell assembly and test electrode (Jones, 1992).

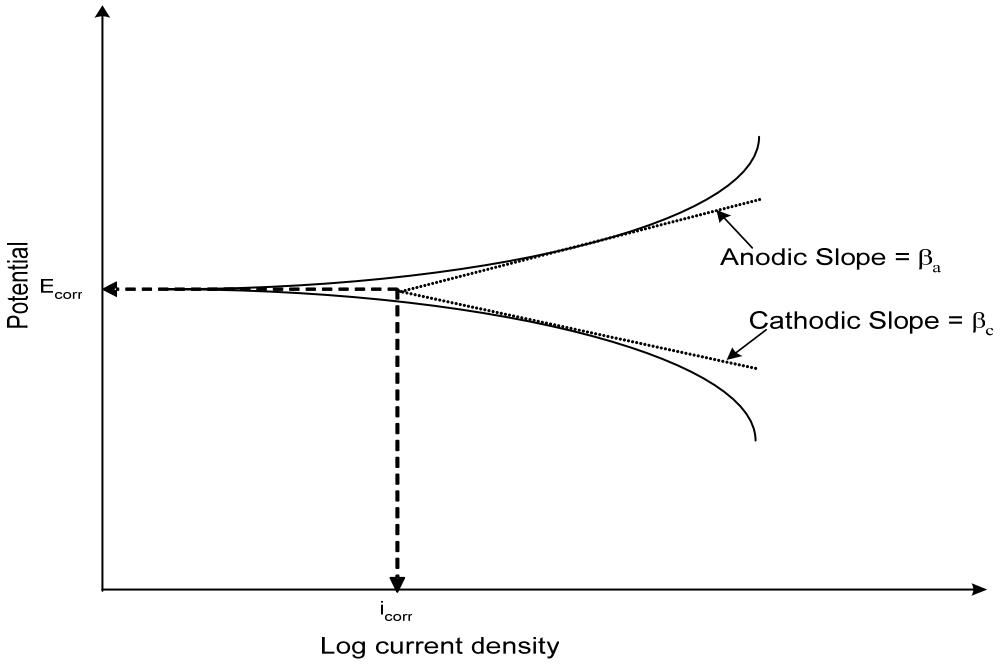

Figure 21: A typical Tafel plot.

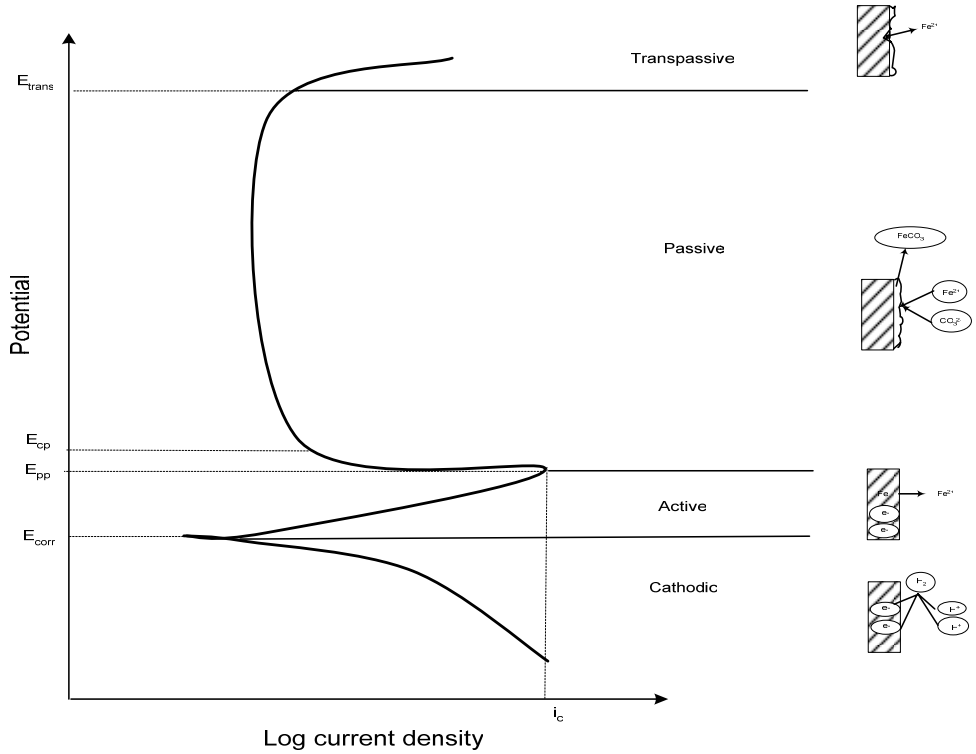

Figure 22: A typical potentiodynamic polarization curve.

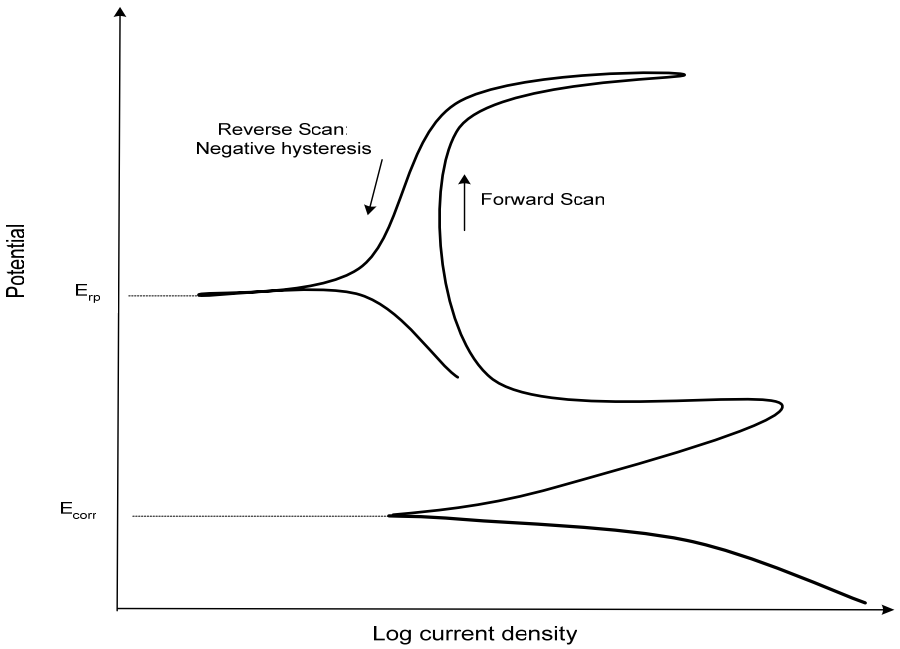

(a) Negative Hysteresis

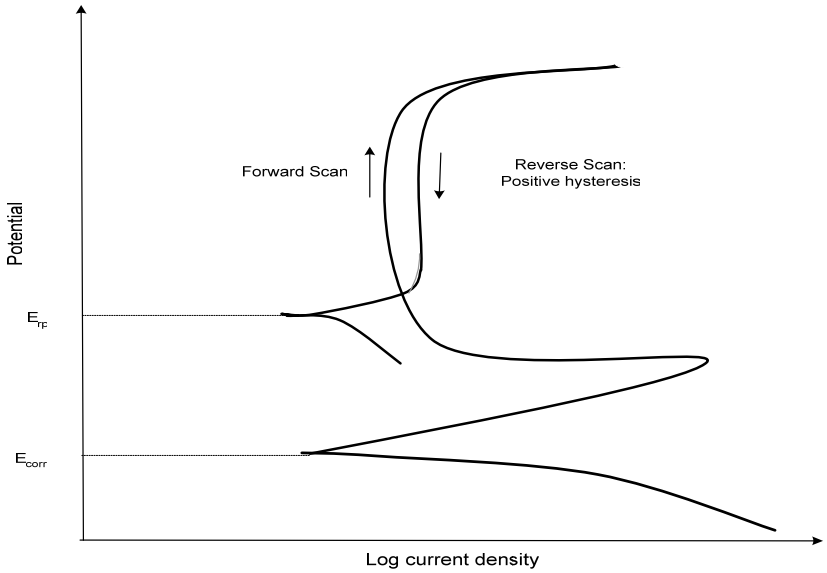

(b) Positive hysteresis

Figure 23: Typical cyclic polarization curve

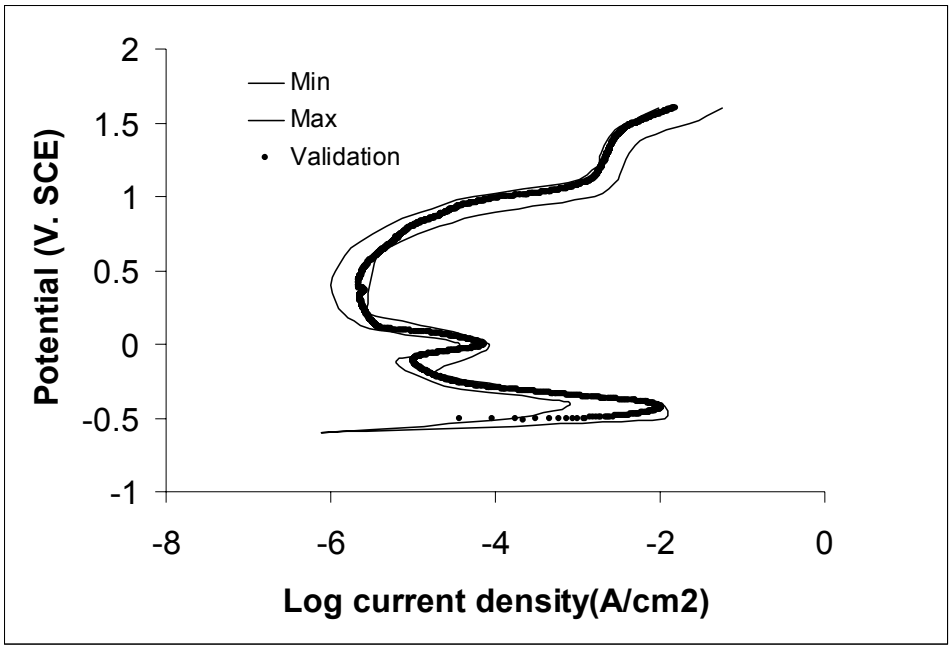

Figure 24: Experimental validation with standard procedure of ASTM G5 (1999).

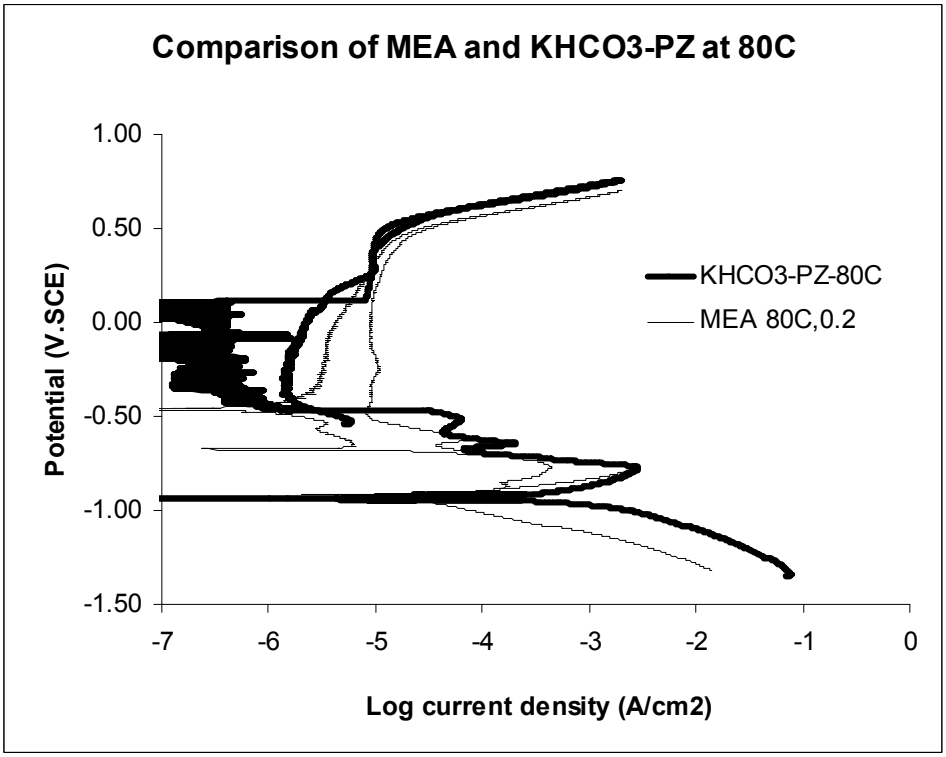

Figure 25: Cyclic polarization curves of carbon steel immersed in 5 molar MEA and 5m.$KHCO_3$-2.5m piperazine at 80^{o}C.

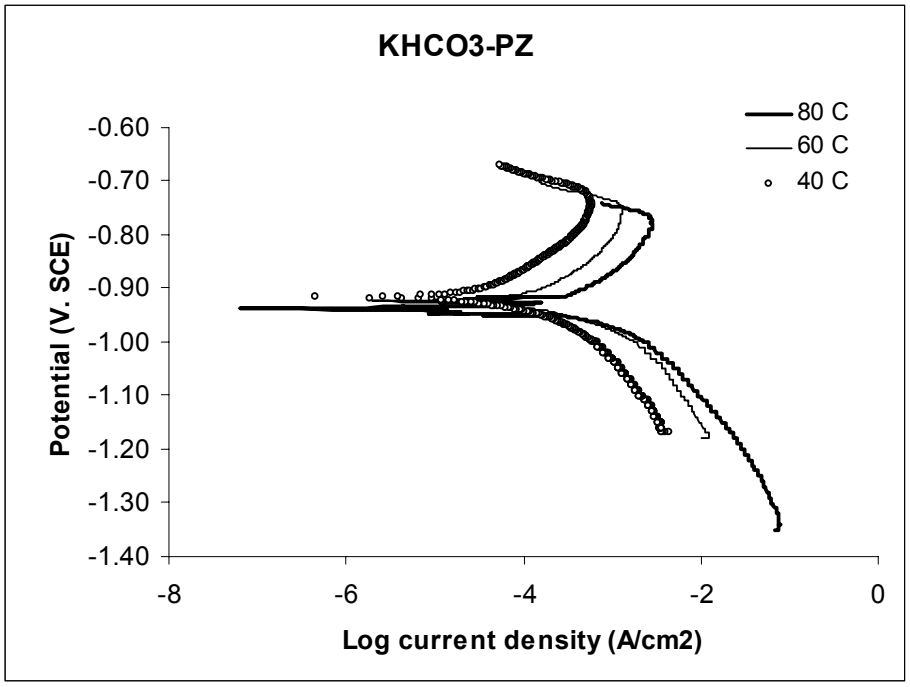

Figure 26: Polarization curves of carbon steel immersed in 5m.$KHCO_3$-2.5m piperazine.

Table 11: pH and conductivity of MEA and $KHCO_3$-piperazine system.

System	pH	Conductivity (mS/cm)
MEA (80^{o}C)	9.11 - 9.17	24.3
$KHCO_3$-PZ (40^{o}C)	10.43 - 10.48	108.6
$KHCO_3$-PZ (60^{o}C)	9.93 - 9.94	118.0 – 118.5
$KHCO_3$-PZ (80^{o}C)	9.34 - 9.53	121.9 – 122.1

References

Bishnoi, S. Carbon dioxide absorption and solution equilibrium in piperazine activated methyldiethanolamine. Ph.D. Dissertation, The University of Texas at Austin, Austin, TX, 2000.

Chen, C., Britt, H.I.; Boston, J.F.; Evans, L.B. Local composition model for excess Gibbs energy of electrolyte systems. Part I: Single solvent, single completely dissociated electrolyte systems. *AIChE J.* 1982, 28, 588-596.

Chen, C. and Evans, L. B. A local composition model for excess Gibbs energy of aqueous electrolyte systems. *AIChE J.* 1986, 32, 444-454.

Cullinane, J.T. "Thermodynamics and kinetics of aqueous piperazine with potassium carbonate for carbon dioxide absorption." Ph.D. Dissertation, Department of Chemical Engineering, The University of Texas at Austin, Austin, TX, 2005.

Dionex IonPac CS16 Analytical Column Product Manual. Revision 03. May 2003. http://www1.dionex.com/en-us/webdocs/manuals/ic/31747-03_CS16_V19.pdf (Accessed January 2005)

Goff, G.S., Rochelle, G.T., "Monoethanolamine Degradation: O_2 Mass Transfer Effects under CO_2 Capture Conditions", *Industrial & Engineering Chemistry Research,* 2004, 43(20), 6400-6408.

Leites, I.L., Berchenko, V.M., "Application of The Second Law of Thermodynamics for Optimization of absorption Processes to Decrease the Energy Consumption", *Proc. International Conf. Energy Systems and Ecology,* 2003, 771-778.

Mock, B.; Evans, L. B.; Chen, C. Thermodynamic representation of phase equilibria of mixed solvent electrolyte systems. *AIChE J.* 1986, 32, 1655-1664.

Onda, K.; Takeuchi, H.; Okumoto, Y. Mass transfer coefficients between gas and liquid phases in packed columns. *J Chem. Eng. Jpn.* 1968, 1.

Oyenekan, B. A., and G. T. Rochelle, "Energy Performance of Stripper Configurations for CO2 Capture by Aqueous Amines," *Industrial & Engineering Chemistry Research,* 45(8), 2457-2464 (2006).

Rochelle, G. T. Personal Communication to Andrew Sexton. Austin, TX, 2005.

Shoulders, B. Personal Communication to Andrew Sexton. Austin, TX, 2005.

Wang, J. Personal Communication to Andrew Sexton. Austin, TX, 2005.

Wilson, I. Gas-liquid contact area of random and structured packing. M.S. Thesis, The University of Texas at Austin, Austin, TX, 2004.